AGU PUBLICATIONS

Paleoceanography

RESEARCH ARTICLE
10.1002/2014PA002717

Key Points:
- We present four reconstructions of regional tropical SSTs based on coral data
- These reconstructions show warming of the tropical oceans beginning in the 1830s
- We find no evidence that external climate forcing altered ENSO activity

Supporting Information:
- Text S1

Correspondence to:
J. E. Tierney,
tierney@whoi.edu

Citation:
Tierney, J. E., N. J. Abram, K. J. Anchukaitis, M. N. Evans, C. Giry, K. H. Kilbourne, C. P. Saenger, H. C. Wu, and J. Zinke (2015), Tropical sea surface temperatures for the past four centuries reconstructed from coral archives, *Paleoceanography*, *30*, 226–252, doi:10.1002/2014PA002717.

Received 8 SEP 2014
Accepted 11 FEB 2015
Accepted article online 16 FEB 2015
Published online 18 MAR 2015

Tropical sea surface temperatures for the past four centuries reconstructed from coral archives

Jessica E. Tierney[1], Nerilie J. Abram[2], Kevin J. Anchukaitis[1], Michael N. Evans[3], Cyril Giry[4], K. Halimeda Kilbourne[3,5], Casey P. Saenger[6], Henry C. Wu[4], and Jens Zinke[7,8]

[1]Woods Hole Oceanographic Institution, Woods Hole, Massachusetts, USA, [2]Research School of Earth Sciences and Centre of Excellence for Climate System Science, Australian National University, Canberra, ACT, Australia, [3]Department of Geology and Earth System Science Interdisciplinary Center, University of Maryland, College Park, Maryland, USA, [4]MARUM–Center for Marine Environmental Sciences, University of Bremen, Bremen, Germany, [5]Chesapeake Biological Laboratory, University of Maryland Center for Environmental Science, Solomons, Maryland, [6]Joint Institute for the Study of the Atmosphere and Ocean, University of Washington, Seattle, Washington, USA, [7]School of Earth and Environment and Australian Institute of Marine Science, Oceans Institute, University of Western Australia, Crawley, Western Australia, Australia, [8]School of Geography, Archaeology and Environmental Studies, University of the Witwatersrand, Johannesburg, South Africa

Abstract Most annually resolved climate reconstructions of the Common Era are based on terrestrial data, making it a challenge to independently assess how recent climate changes have affected the oceans. Here as part of the Past Global Changes Ocean2K project, we present four regionally calibrated and validated reconstructions of sea surface temperatures in the tropics, based on 57 published and publicly archived marine paleoclimate data sets derived exclusively from tropical coral archives. Validation exercises suggest that our reconstructions are interpretable for much of the past 400 years, depending on the availability of paleoclimate data within, and the reconstruction validation statistics for, each target region. Analysis of the trends in the data suggests that the Indian, western Pacific, and western Atlantic Ocean regions were cooling until modern warming began around the 1830s. The early 1800s were an exceptionally cool period in the Indo-Pacific region, likely due to multiple large tropical volcanic eruptions occurring in the early nineteenth century. Decadal-scale variability is a quasi-persistent feature of all basins. Twentieth century warming associated with greenhouse gas emissions is apparent in the Indian, West Pacific, and western Atlantic Oceans, but we find no evidence that either natural or anthropogenic forcings have altered El Niño–Southern Oscillation-related variance in tropical sea surface temperatures. Our marine-based regional paleoclimate reconstructions serve as benchmarks against which terrestrial reconstructions as well as climate model simulations can be compared and as a basis for studying the processes by which the tropical oceans mediate climate variability and change.

1. Introduction

Global- and regional-scale climate reconstructions of last millennium temperature changes are largely based on terrestrial paleoclimate proxy data [*Past Global Changes* (*PAGES*) *2k Consortium*, 2013; *Masson-Delmotte et al.*, 2013]. However, 70% of Earth's surface area is ocean, and changes in oceanic circulation and associated latent and sensible heat fluxes cause and respond to global-scale climate variations. The tropical oceans cover only about one quarter of the total surface area equatorward of 30°, but because of their high heat content, ocean-atmosphere coupling, and potential for large interannual and longer-term variations [*Gill and Rasmusson*, 1983; *Fedorov and Philander*, 2000], they are an important part of the internal variability of the climate system [*Newman et al.*, 2003]. Inferences on past changes in oceanic climate that are derived from reconstructions based on both terrestrial and marine observations [e.g., *Mann et al.*, 2009; *Emile-Geay et al.*, 2013a, 2013b] rely on the assumption that land-sea climatic teleconnections are time stationary, but this may not be the case [e.g., *Cole and Cook*, 1998; *Kumar and Hoerling*, 1998; *Gershunov and Barnett*, 1998; *Rajagopalan et al.*, 2000; *Diaz et al.*, 2001; *Knippertz et al.*, 2003; *van Oldenborgh*, 2005; *López-Parages and Rodríguez-Fonseca*, 2012; *Gallant et al.*, 2013]. Systematic tests of climate field reconstruction methods also suggest that remote interpolations into unobserved (largely oceanic) regions carry large uncertainties [*Smerdon et al.*, 2011]. This highlights the need for reconstructions of marine climate derived solely from marine paleoclimate data, in order to better assess the relative importance of internally and externally forced climate variations on the ocean. Furthermore, independent estimates of past marine and terrestrial

climate are needed in order to evaluate and test hypotheses about the pattern, strength, and stability of ocean-atmosphere teleconnections in time and space [c.f. *Mullan*, 1995; *Cole and Cook*, 1998; *Gershunov and Barnett*, 1998; *Dommenget et al.*, 2012; *Gallant et al.*, 2013].

Corals represent one of our best high-resolution in situ archives of tropical ocean variability in the recent past [*Lough*, 2010], but with a few notable exceptions [e.g., *Evans et al.*, 2002; *Wilson et al.*, 2006] paleoclimate data from tropical coral archives are not often employed as the sole data source for reconstructions of past ocean conditions. A number of different analyses can be made on massive, aragonitic, stony corals that allow for paleotemperature estimation [*Dunbar and Cole*, 1999; *Gagan et al.*, 2000; *Lough*, 2010]. The most common is the oxygen isotopic composition (δ^{18}O) of coral carbonate, whose variations are negatively proportional to the temperature of calcification [*Weber and Woodhead*, 1972; *Grossman and Ku*, 1986] and positively proportional to variations in seawater δ^{18}O [*Fairbanks et al.*, 1997]. The δ^{18}O of seawater may be modified by evaporation, precipitation, advection, convection, and turbulent mixing [*LeGrande and Schmidt*, 2006]. At some locations, local variation in seawater δ^{18}O is large and dominates the coral δ^{18}O signature [*Cole et al.*, 1993]. As a result, the use of δ^{18}O data for reconstruction of sea surface temperature must be carefully considered [*Evans et al.*, 2000]. The incorporation of strontium (Sr) into coral aragonite, measured by the skeletal Sr/Ca ratio, also varies in negative proportion with calcification temperature [*Kinsman and Holland*, 1969; *de Villiers et al.*, 1994]. When paired with δ^{18}O observations, Sr/Ca observations can in theory allow for estimation of the seawater δ^{18}O contribution [*McCulloch et al.*, 1994; *Gagan et al.*, 1998; *Nurhati et al.*, 2011]. However, biological "vital" effects and skeletal growth processes may confound interpretations of both coral Sr/Ca and δ^{18}O [*Cohen et al.*, 2001; *Cobb et al.*, 2003; *Linsley et al.*, 2006; *Gagan et al.*, 2012; *Juillet-Leclerc et al.*, 2014]. A third important category of coral-derived paleoenvironmental data is coral growth rate, as measured by linear extension or calcification rate [*Lough and Barnes*, 1997; *Lough and Cooper*, 2011]. Coral skeletal growth varies more generally with the optimality of growing conditions [*De'ath et al.*, 2009; *Lough and Cooper*, 2011; *Cooper et al.*, 2012], of which temperature can exert a positive [*Lough and Cooper*, 2011] or negative [*Saenger et al.*, 2009] control.

Individual coral records generally show a high level of fidelity in capturing seasonal to interannual climate variability in their geochemical signals [e.g., *Felis et al.*, 2004; *Giry et al.*, 2012]. Because coral extension rates are generally thought to be relatively constant throughout the year except under extreme conditions [*Lough and Cooper*, 2011], seasonal growth biases arising from uniform sampling of the archive are believed to be minimal at most locations. In locations where seasonally suboptimal conditions do have the potential to bias coral growth toward a particular season [e.g., *DeLong et al.*, 2014], this can be ameliorated by using monthly to seasonal sampling and intraannual age modeling to yield records that are representative of the annual mean [*Quinn et al.*, 1996; *Leder et al.*, 1996; *Quinn et al.*, 1998; *Evans et al.*, 2000; *Swart et al.*, 2002]. The reliability of secular trends and mean climate changes derived from individual coral colonies is more difficult to assess, because intercolony differences arise from localized environmental conditions, diagenetic alteration of coral aragonite [*McGregor and Gagan*, 2003; *Hendy et al.*, 2007; *McGregor and Abram*, 2008], and chronological uncertainty [*Evans et al.*, 1999; *Comboul et al.*, 2014]. These uncertainties can be partly overcome by using replication from multiple coeval coral colonies [*Lough*, 2004; *Abram et al.*, 2009; *Pfeiffer et al.*, 2009; *DeLong et al.*, 2013]. Furthermore, such influences should be largely independent across colonies, sites, and regions, such that the composite of multiple records at broad spatial scales should enhance common, regional-scale climatic variations and improve detection of secular climate changes [*Evans et al.*, 2002; *Wilson et al.*, 2010].

Here as part of the international, community-based, and ongoing Ocean2k subgroup of the Past Global Changes (PAGES) 2k Consortium (http://www.pages-igbp.org/workinggroups/2k-network), we present annually resolved, basin-scale reconstructions of tropical sea surface temperature (SST) anomalies based solely on seasonal to annual resolution data from coral archives. We focus on four regions where data availability permits the reconstruction of regionally averaged SST anomalies: the western Atlantic, the eastern Pacific, the western Pacific, and the Indian Oceans (Figure 1). We estimate uncertainty and the interpretability of the results through ensemble calibration and validation exercises. We analyze the spectral characteristics of the results, estimate the timing of the onset of recent significant warming trends in the tropical oceans, and discuss the influence of well-mixed greenhouse gases and solar and volcanic activity on reconstructed tropical SSTs.

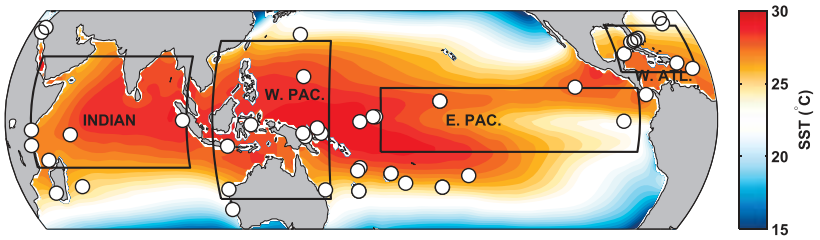

Figure 1. Map of the four regions targeted for reconstruction (black rectangles), and the locations of the proxies (white circles) that comprise the reconstructions, superimposed on mean annual climatological sea surface temperatures [*Locarnini et al.*, 2010]. The tropical SST reconstruction regions cover the Indian (20°N–15°S, 40–100°E), western Pacific (25°N–25°S, 110–155°E), eastern Pacific (10°N–10°S, 175°E–85°W), and western Atlantic (15–30°N, 60–90°W) oceans.

2. Materials and Methods

2.1. Proxy Data

The paleoenvironmental data used to develop the reconstructions comprise published, publicly available data that meet the following criteria: (1) the data are derived from a marine coral archive; (2) they vary in response to changes in temperature, based on a priori biological, physical, or chemical studies—this excludes, for example, trace elements or luminescence changes that are indicative of changes in terrestrial runoff [e.g., *Isdale et al.*, 1998; *Lough et al.*, 2002; *McCulloch et al.*, 2003] as well as growth records where temperature is not unambiguously the primary control on coral extension rate [e.g., *De'ath et al.*, 2009; *Cooper et al.*, 2012]; (3) the average chronological resolution of the data is at least annual; (4) individual records contain sufficient data (more than 80 contiguous years) during the twentieth century, to enable meaningful calibration and validation; and (5) individual records contain data prior to 1900 A.D., such that they contribute to the reconstruction of SSTs before the historical period of direct observations. Table 1 lists the data sets that meet these criteria as of September 2014, including their location, data type, record length, source reference, and assignment to reconstruction target (section 2.3). At some sites, the same proxy measurement was made on multiple coral specimens and then standardized and composited into a single record, either by the original authors or as part of this study. Such sites are marked accordingly in Table 1. Some locations also offer multiple data types, typically δ^{18}O and Sr/Ca. In these cases, we treated each time series as a separate record for inclusion in the reconstruction, for although they are often measured on the same coral cores and therefore may not be spatially, temporally, or sample independent, the data provide geochemically independent estimates of SST. Two sites required manual adjustment of the data prior to use in the reconstruction. The first is the data set from Urvina Bay, Galápagos, which consists of δ^{18}O data from two different coral species. Following the procedure of the original publication [*Dunbar et al.*, 1994], we adjusted the δ^{18}O data from species *Pavona gigantea* (core UR-87) by 0.40‰ to match the mean of the data from species *Pavona clavis* (core UR-86). The second is the data set from Nauru Island, which consists of a composite of two cores. *Guilderson and Schrag* [1999] inferred that the δ^{18}O data from cores Nauru-1 and Nauru-2 are overprinted by kinetic isotope effects related to relatively low extension rates prior to year 1896 and year 1939, respectively; therefore, we removed these data from the time series.

As the original data time series vary in their temporal resolution from monthly to annual, we downsampled subannually resolved data series by binning data into April–March annual averages [*Evans et al.*, 2002]. The April–March "tropical" year was chosen to minimize the splitting of tropical interannual climate events (such as those associated with the El Niño–Southern Oscillation (ENSO)) across adjacent annual increments [*Ropelewski and Halpert*, 1987; *Evans et al.*, 2000, 2002]. Therefore, in the resulting reconstructions, year 1982 (for example) refers to April 1982 to March 1983.

2.2. Instrumental Data

As a basis for the reconstruction targets, against which the paleoclimate data are calibrated, we used April–March annual averages of the Hadley Centre's HadISST-gridded SST product at $1° \times 1°$ resolution, expressed as anomalies relative to the 1961–1990 reference period [*Rayner et al.*, 2003]. HadISST is an interpolated product that makes statistical assumptions to infer SSTs for grid points and time points with missing data. Inferred SSTs are particularly dependent on the interpolation method in the late nineteenth and early twentieth centuries, when observations in the tropical oceans—particularly in the Pacific and Indian—are sparse [c.f. *Kaplan et al.*, 1998; *Rayner et al.*, 2006; *Yasunaka and Hanawa*, 2011]. We tested the sensitivity of

AGU Paleoceanography

Table 1. List of the Sites and Coral Paleoclimate Data Used in This Study[a]

Region	Site Name	Latitude	Longitude	Record Length	Resolution	Proxy	*r*, Site SST Versus Target	*r*, Proxy Versus Target	*p* Value	Weight	Reference
Western Pacific	Chichijima	27.1	142.2	1873–1994	subseasonal	Sr/Ca	0.57	0.33	0.08	0	*Felis et al.* [2009]
	Chichijima	27.1	142.2	1873–1994	subseasonal	$\delta^{18}O$	0.58	0.14	0.46	0	*Felis et al.* [2009]
	Double Reef	13.6	144.83	1790–2000	monthly	$\delta^{18}O$	0.85	−0.58	0.0007	0.58	*Asami et al.* [2005]
	Bali	−8.2573	115.5757	1782–1990	monthly	$\delta^{18}O$	0.75	−0.42	0.005	0.42	*Charles et al.* [2003]
	Bunaken	−1.5	124.833	1860–1990	monthly	$\delta^{18}O$	0.85	−0.57	0	0.57	*Charles et al.* [2003]
	Moorea	−17.5	−149.83	1852–1990	annual	$\delta^{18}O$	0.51	−0.48	0	0.48	*Boiseau et al.* [1998, 1999]
	Madang	−5.2167	145.8167	1880–1993	seasonal	$\delta^{18}O$	0.73	−0.27	0.09	0.25	*Tudhope et al.* [2001]
	Laing	−4.15	144.8833	1884–1993	seasonal	$\delta^{18}O$	0.75	−0.62	0	0.62	*Tudhope et al.* [2001]
	Kavieng	−2.5	150.5	1823–1997	monthly	Sr/Ca	0.75	−0.25	0.22	0.19	*Alibert and Kinsley* [2008]
	Rabaul	−4.18	151.98	1867–1998	monthly	$\delta^{18}O$	0.74	−0.24	0.09	0.22	*Quinn et al.* [2006]
	Rabaul	−4.18	151.98	1867–1998	monthly	Sr/Ca	0.74	0.12	0.54	0	*Quinn et al.* [2006]
	Rarotonga[b]	−21.2378	−159.8278	1727–1996	subseasonal	$\delta^{18}O$	0.49	−0.46	0.0005	0.46	*Linsley et al.* [2006]
	Rarotonga[b]	−21.2378	−159.8278	1727–1996	subseasonal	Sr/Ca	0.49	−0.15	0.37	0.10	*Linsley et al.* [2006]
	Espiritu Santo	−15	166.99	1807–1979	annual	$\delta^{18}O$	0.67	0.23	0.09	0	*Quinn et al.* [1996]
	Sabine Bank[b]	−15.94	166.04	1842–2007	monthly	$\delta^{18}O$	0.67	−0.31	0.04	0.30	*Gorman et al.* [2012]
	Amedee Island[b]	−22.29	166.27	1649–1999	monthly	Sr/Ca	0.70	−0.41	0.0004	0.41	*DeLong et al.* [2012, 2013]
	Amedee Island	−22.48	166.47	1657–1992	seasonal	$\delta^{18}O$	0.70	−0.31	0.13	0.27	*Quinn et al.* [1998]
	Savusavu Bay	−16.82	179.23	1776–2001	annual	$\delta^{18}O$	0.52	−0.16	0.46	0.09	*Bagnato et al.* [2005]
	Savusavu Bay[b]	−16.8167	179.2333	1617–2001	annual	$\delta^{18}O$	0.52	−0.28	0.09	0.26	*Linsley et al.* [2006]
	Savusavu Bay	−16.8167	179.2333	1782–1996	annual	Sr/Ca	0.52	−0.27	0.04	0.26	*Linsley et al.* [2006]
	Ningaloo Reef	−21.905	113.965	1878–1995	subseasonal	$\delta^{18}O$	0.76	−0.57	0.0001	0.57	*Kuhnert et al.* [2000]
	Abraham Reef	−22.1	153	1638–1983	annual	$\delta^{18}O$	0.84	0.04	0.77	0	*Druffel and Griffin* [1999]
	Tonga	−19.9	−174.7	1792–2004	annual	Sr/Ca	0.58	−0.32	0.10	0.29	*Wu et al.* [2013]
Eastern Pacific	Clipperton Atoll[b]	10.2773	−109.2131	1893–1994	subseasonal	$\delta^{18}O$	0.89	−0.44	0	0.44	*Linsley et al.* [2000]
	Urvina Bay[b]	−0.4	−91.23	1607–1981	annual	$\delta^{18}O$	0.84	−0.49	0	0.49	*Dunbar et al.* [1994]
	Maiana Atoll	1	173	1840–1994	subseasonal	$\delta^{18}O$	0.84	−0.65	0	0.65	*Urban et al.* [2000]
	Tarawa Atoll	1	172	1894–1990	monthly	$\delta^{18}O$	0.82	−0.69	0	0.69	*Cole and Fairbanks* [1990] and *Cole et al.* [1993]
	Nauru[b]	−0.533	166.9283	1897–1995	subseasonal	$\delta^{18}O$	0.66	−0.51	0	0.51	*Guilderson and Schrag* [1999]
	Secas Island	7.95	−82	1707–1984	subseasonal	$\delta^{18}O$	0.82	−0.10	0.34	0.07	*Linsley et al.* [1994]
	Palmyra Atoll[b]	5.87	−162.13	1928–1998 (discontinuous)	monthly	$\delta^{18}O$	0.92	−0.71	0	0.71	*Cobb et al.* [2003]
	Palmyra Atoll	5.87	−162.13	1886–1998	monthly	Sr/Ca	0.92	−0.48	0	0.48	*Nurhati et al.* [2009, 2011]

10.1002/2014PA002717

10.1002/2014PA002717

Table 1. (continued)

Region	Site Name	Latitude	Longitude	Record Length	Resolution	Proxy	*r*, Site SST Versus Target	*r*, Proxy Versus Target	*p* Value	Weight	Reference
Indian	Malindi	−3	40	1801–1994	annual	$\delta^{18}O$	0.91	−0.53	0.007	0.53	*Cole et al.* [2000]
	Mayotte	−12.65	45.1	1865–1994	subseasonal	$\delta^{18}O$	0.91	−0.49	0.001	0.49	*Zinke et al.* [2008, 2009]
	Mayotte	−12.65	45.1	1865–1994	subseasonal	Sr/Ca	0.91	−0.25	0.04	0.24	*Zinke et al.* [2008, 2009]
	Ifaty Reef	−23.15	43.58	1659–1995	subseasonal	$\delta^{18}O$	0.76	−0.09	0.64	0.03	*Zinke et al.* [2004]
	Houtman Abrolhos	−28.4617	113.7683	1794–1994	subseasonal	$\delta^{18}O$	0.61	−0.19	0.15	0.16	*Kuhnert et al.* [1999]
	Mafia Island	−8.0167	39.5	1622–1722 and 1896–1998	subseasonal	$\delta^{18}O$	0.92	−0.55	0	0.55	*Damassa et al.* [2006]
	Mentawai[b]	−0.13	98.52	1858–1998	monthly	$\delta^{18}O$	0.90	−0.55	0.0008	0.55	*Abram et al.* [2008]
	Mahe, Seychelles	−4.62	55	1846–1995	monthly	$\delta^{18}O$	0.91	−0.58	0	0.58	*Charles et al.* [1997]
	Malindi	−3.2	40.1	1887–2002	monthly	$\delta^{18}O$	0.91	−0.45	0.002	0.45	*Nakamura et al.* [2009]
	La Réunion	−21	55	1832–1995	subseasonal	$\delta^{18}O$	0.76	−0.49	0.005	0.48	*Pfeiffer et al.* [2004]
	Aqaba[b]	29.4333	34.9667	1788–1992	annual	$\delta^{18}O$	0.59	−0.28	0.11	0.25	*Heiss* [1994]
	Ras Um Sidd[b]	27.8483	34.31	1897–1993	subseasonal	$\delta^{18}O$	0.58	−0.43	0.04	0.41	*Moustafa* [2000]
	Ras Um Sidd	27.85	34.32	1750–1995	subseasonal	$\delta^{18}O$	0.58	−0.28	0.11	0.25	*Felis et al.* [2000]
Atlantic	Bermuda	30.6486	−64.9888	1781–1998	annual	$\delta^{18}O$	0.74	0.13	0.17	0	*Goodkin et al.* [2008]
	Bermuda	30.6486	−64.9888	1781–1998	annual	Sr/Ca	0.74	−0.39	0.17	0.32	*Goodkin et al.* [2008]
	Guadeloupe	16.2	−61.49	1895–1999	monthly	$\delta^{18}O$	0.83	−0.14	0.14	0.12	*Hetzinger et al.* [2010]
	Guadeloupe	16.2	−61.49	1895–1999	monthly	Sr/Ca	0.83	−0.29	0.46	0.16	*Hetzinger et al.* [2010]
	Puerto Rico	17.93	−67	1751–2004	annual	$\delta^{18}O$	0.88	−0.29	0.02	0.29	*Kilbourne et al.* [2008]
	Puerto Rico	17.93	−67	1751–2004	annual	Sr/Ca	0.88	0.10	0.33	0	*Kilbourne et al.* [2008]
	Bermuda	32.467	−64.7	1825–1983	monthly	$\delta^{18}O$	0.69	−0.11	0.37	0.07	*Kuhnert et al.* [2005]
	Bermuda	32.467	−64.7	1825–1983	monthly	Sr/Ca	0.69	0.29	0.28	0	*Kuhnert et al.* [2005]
	Florida Bay	24.93	−80.75	1824–1985	annual	$\delta^{18}O$	0.73	0.01	0.94	0	*Swart et al.* [1996a]
	Biscayne National Park, Florida	25.38	−80.17	1751–1986	annual	$\delta^{18}O$	0.70	−0.08	0.51	0.04	*Swart et al.* [1996b]
	Bahamas	25.84	−78.62	1552–1991	annual	growth rate	0.80	−0.59	0.006	0.59	*Saenger et al.* [2009]
	Yucatan[b]	20.83	−86.74	1773–2009	annual	growth rate	0.88	−0.72	0	0.72	*Vásquez-Bedoya et al.* [2012]
	Dry Tortugas[b]	24.66	−82.83	1734–2008	monthly	Sr/Ca	0.74	−0.02	0.94	0.001	*DeLong et al.* [2014]

[a]Correlations denote the Pearson correlation between the time series and mean annual target region Hadley Centre Global Sea Ice and Sea Surface Temperature (HadISST), 1900–1990. The *p* values indicate the significance level as determined by a nonparametric Monte Carlo process [*Ebisuzaki*, 1997]. Weights correspond to $r(1-p)$ or are set to zero when the direction of correlation with target SSTs is physically implausible.

[b]Sites with multiple composited cores.

our results to our choice of instrumental SST product by repeating the reconstructions with observational targets derived from Extended Reconstructed Sea Surface Temperature (ERSST) v3b [*Smith et al.*, 2008], which makes different assumptions regarding bias correction and interpolation and can therefore result in different early twentieth century estimates as well as inferred long-term trends [*Emile-Geay et al.*, 2013a].

2.3. Reconstruction Targets

Based on paleoclimate data availability, we reconstruct area-mean SST anomalies in four tropical ocean regions (Figure 1). These four targets were chosen based on their proximity to the coral sampling sites and through analysis of spatial temperature covariance to ensure that SST variability within the target was a homogeneous representation of regional variability. For example, the boundaries of the western Pacific (25°N–25°S, 110°E–155°E) and eastern Pacific (10°N–10°S, 175°W–85°W) targets were chosen to avoid conflation of opposite-sign SST variations associated with ENSO. In the tropical Indian Ocean, for annually averaged data the basin-wide SST signal is larger than the seasonally restricted Indian Ocean Dipole (IOD) variability; hence, we reconstruct a basin-wide target (20°N–15°S, 40°E–100°E). The proxy network also allows for reconstruction of SSTs in the tropical western Atlantic (30°N–15°N, 90°W–60°W). Here the target box is restricted to the Caribbean region, where the majority of the existing proxy data are found.

The chosen targets are a necessary compromise in order to reconstruct SSTs at a regional scale but inevitably leave some paleoclimate data locations outside of the target box (Figure 1). Also, regional targets may not capture site-local signals. To assess the expected relationship between the proxy sites and the targets, we report the correlation between the nearest HadISST grid cell to each site and the regional target in Table 1. While, in general, the correlations are high, indicating that our target regions and coral sites are reasonable representations of the large-scale SSTs, in certain regions they are systematically lower. The South Pacific region, for example, lies outside the western Pacific target box (Figure 1), and while variability in that region is correlated to the SSTs in the target, the correlations overall tend to be lower (approximately $r = 0.5$, see Table 1). Similarly, the Red Sea coral locations have a lower correlation (approximately $r = 0.6$) with the Indian Ocean target.

Note that each proxy data series was uniquely assigned to a single target region: no series were used for reconstruction of more than one target (Table 1). The resulting targets (Figure 1) correspond to a large fraction of the tropical oceans and include regions important for air-sea interaction and for which interdecadal and secular SST changes both large and small have been observed in the twentieth century [e.g., *Gill*, 1982; *Bottomley et al.*, 1990; *Trenberth and Hurrell*, 1994; *Parker et al.*, 1994].

2.4. Reconstruction Method

We used a weighted, composite-plus-scale (CPS) approach to reconstruct regionally averaged SST histories for the four target regions. The CPS approach follows previous reconstruction efforts [*Esper et al.*, 2002, 2005; *Wilson et al.*, 2006, 2010; *Emile-Geay et al.*, 2013a, 2013b] and uses a nesting procedure [*Meko*, 1997; *Cook et al.*, 1999, 2002] to account for the effect of the changing number of available observations on reconstructed skill and variance over time. Rather than prescreening the paleoclimate data for significant correlations with the SST targets and eliminating time series that fall below a particular significance threshold [e.g., *Wilson et al.*, 2010; *Emile-Geay et al.*, 2013a], we opted instead to employ a weighting procedure to scale the contribution of each record to the composite by their relationship with the instrumental target SST [e.g., *Hegerl et al.*, 2007; *Cook et al.*, 2010]. The weight applied is the Pearson product-moment correlation coefficient (r) between each paleoclimate time series and target SST anomalies from 1900 to 1990 A.D. (or 1900 to most recent year for time series that only reach the 1980s), multiplied by $1 - p$, where p is the p value of the correlation accounting for serial correlation [*Ebisuzaki*, 1997]. Thus, the data are scaled by both the magnitude and significance of variance shared with the target. These correlation statistics are calculated without the use of linear detrending of the paleoclimate or instrumental data in order to consider long-term trends. Data with a correlation of zero, or a correlation whose sign is not in agreement with that expected a priori from biophysical or experimental understanding of the proxy response to climate (see section 2.1), were assigned a weight of zero and therefore are effectively excluded from contributing to the CPS reconstruction. While the analyses are derived from the reconstructions based on the $r(1 - p)$ weighting scheme, we also tested the sensitivity of the reconstruction results to the weighting choice by performing reconstructions using no weighting (r^0, but with the records with a zero or opposite-signed correlation still excluded) and a variance $r^2(1 - p)$ weighting.

For each nest, the paleoclimate data are standardized (mean set to zero and standard deviation set to 1) and then composited into their weighted average. The mean and standard deviation of the resulting composite is then scaled to that of the calibration period, and the nests are spliced together to form the complete reconstruction [c.f. *Esper et al.*, 2002; *Emile-Geay et al.*, 2013b]. Skill statistics are calculated over the validation period for each nest, including the coefficient of determination (r^2), the reduction of error (RE), and the coefficient of efficiency (CE) [*Cook et al.*, 1999]. Values of RE (CE) above zero indicate some statistical skill in that the error variance of the reconstruction in the validation period is less than observed SST variance within the calibration (validation) period.

The calibration period was defined as the contiguous two thirds of the years that the paleoclimate data and instrumental time series share in common, with the validation period comprising the remaining one third. In addition, for nests of paleoclimate data that extend farther into the present (i.e., dates more recent that the most recent year of the contiguous calibration period), this interval of time was used as an extra validation interval. This ensures, for example, that a single older data time series (e.g., that ends in 1985) does not prevent the reconstruction from being validated against more modern data (e.g., 1985–2000). To assess the sensitivity of the reconstruction to the choice of calibration period [e.g., *Frank et al.*, 2010; *Anchukaitis et al.*, 2013], we progressively stepped the calibration window by 5 year intervals across the common-year period, using the remaining common-year data (as well as "extra" modern years, if applicable) for validation. We note that because the CPS method sets the reconstruction mean to match the calibration period mean, this does not necessarily result in a zero mean from 1961 to 1990. We also tested the sensitivity of the reconstruction to inclusion of individual time series by systematically leaving each record out and then recalculating the reconstruction. From these iterations, we generated an ensemble of reconstructions for each target region that samples these two sources of uncertainty in the CPS method. We designated the reconstruction ensemble member with the highest time-integrated cumulative RE score (and that has an RE > 0 over the validation period) as the "best" reconstruction and estimate its accuracy from its validation period root-mean-square error (RMSE). We report the validation skill statistics for the best reconstruction as well as the median estimates of RE, CE, and r^2 for the full ensemble. We performed statistical analyses on both the best reconstruction and the full ensemble in order to account for reconstruction uncertainty in our interpretations.

2.5. Statistical Analyses

To identify and analyze significant trends in our reconstructions, we used the Significant Zero crossings of derivatives (SiZer) method [*Chaudhuri and Marron*, 1999]. SiZer fits a family of variable width Gaussian filters to the data and searches for the starting and ending points of significant trends, which are defined as the point at which the null hypothesis of no trend can be rejected at the level of $p < 0.1$. We plot the direction and significance of trends to show the influence of different levels of smoothing on the interpretation of change points in the SST reconstructions. For each iteration of the SST reconstructions in each region, we determine the median timing of the most recent transition to significant ($p < 0.1$) warming across all filter widths from 15 to 50 years; we omitted 5 to 14 year filters because of the dominant influence of interannual to decadal climate variability on trend changes at these short smoothing lengths. We then compile this information for each target region to examine the distribution of warming change points across all iterations of the SST reconstructions and determine an overall median timing for the initiation of recent significant warming.

We estimated the power spectral density of each SST reconstruction ensemble member, as well as the corresponding observational data, using the multitaper method [*Thomson*, 1982] and $k = 5$ tapers. The ensemble spectral spread provides an estimate of the uncertainty associated with the reconstruction methods and data, while confidence intervals on individual spectra were calculated using a chi-square approach [*Percival and Walden*, 1993]. In order to observe changes over time in the power spectral density, we conducted an evolutionary multitaper spectral analysis [*Priestley*, 1965] on the best reconstructions for each target region, using a 50 year window and advancing the window in 1 year increments along the length of the reconstructions. To further isolate and observe variability specific to ENSO-type (interannual) and multidecadal frequency bands, we applied a seven-point 3–7 year Butterworth band-pass filter and a seven-point 20–80 year Butterworth band-pass filter, respectively, to the best reconstructions.

3. Results

For each of the four target regions, respectively, we discuss the major features of the reconstructions, their reconstruction skill, and the influence of individual proxy records on the results.

3.1. Indian Ocean

The Indian Ocean regional reconstruction is based on up to 13 coral records and spans the period from 1621 to 2001 (Figure 2a). A map of the weights assigned to each proxy (Figure 3a) shows that records from the equatorial regions of the Indian Ocean contribute most heavily to the reconstruction. A field correlation between the best reconstruction (see section 2.4 for description of how this was identified) indicates that our reconstruction predominantly represents SST variability in the northern and western parts of the target region (Figure 3a). Ensemble statistics suggest reconstruction skill back to the late eighteenth century based on the RE score; however, there are no ensemble members with CE scores greater than zero prior to the 1840s.

The median values of the reconstruction statistics suggest some skill throughout most of the 1621 to 2001 time span, with the exception of 1858–1886, during which the median RE drops below zero (Figure 2a). There are, however, some ensemble members that have high RE during this period; these iterations are those that omit the δ^{18}O record from the northern Mentawai Islands in the eastern Indian Ocean [*Abram et al.*, 2008]. RE is higher for these iterations because, although the overall trend in the Mentawai coral is in agreement with the other tropical Indian Ocean time series, its interannual variability (associated largely with the eastern pole of the IOD) is out of phase. In particular, the Mentawai coral record has large positive δ^{18}O (cooling) excursions during 1877, 1961, 1994, and 1997 associated with positive IOD events, during which times our target SST region shows warming. Hence, its exclusion from the nest starting in 1858 improves reconstruction skill. Likewise, CE is positive from 1846 to 1998 for some iterations that exclude the Mentawai coral, but negative otherwise (Figure 2a). For most of the seventeenth and eighteenth centuries, RE and r^2 values are low, indicating substantially reduced skill, in this case as the number of available records decreases. Furthermore, many of the records that contribute to the reconstruction during this earliest period (δ^{18}O data from Ifaty Reef, Aqaba, and Ras Um Sidd) are only weakly correlated with mean SST in the Indian Ocean target region (Table 1).

The best reconstruction for the Indian Ocean excludes the Mentawai δ^{18}O record, is calibrated on an early period (1897–1960), and is most robust (positive RE and CE) from 1840 to 2001. Decadal and longer-term variations should be interpreted with caution from 1621 to 1839, when CE values are below zero (Figure 2a). According to this reconstruction, the warmest decade of the last circa 400 years was 1986–1995, and the coolest decade was 1833–1842. During these years, the ensemble of SST reconstructions indicate that temperatures were on average 1.0°C cooler than the 1961–1990 mean (Figure 2a). This cooling event is most prominent in the coral δ^{18}O record from La Réunion [*Pfeiffer et al.*, 2004], and may possibly be influenced by local or potentially nontemperature environmental influences. Analysis of the reconstruction ensemble confirms that omission of this record produces a smaller (−0.7°C)—though still cold—anomaly during this epoch. An early to midnineteenth century SST minimum is a feature of all the Indian Ocean ensemble reconstructions, indicating that conditions were 0.8°C cooler than the 1961–1990 mean during the early 1800s (1807–1816). Multiple data series show this cooling, suggesting that it is a robust feature. We note, however, that all of the coral records spanning the early nineteenth century are δ^{18}O data and therefore could also reflect an additional influence of changes in seawater δ^{18}O [*Cole et al.*, 2000; *Pfeiffer et al.*, 2004; *Zinke et al.*, 2009].

3.2. Western Pacific

The western Pacific reconstruction is based on up to 18 coral records and spans the period from 1617 to 2006 (Figure 2b). The reconstruction ensemble demonstrates positive RE values throughout, indicating skill through time and across reconstruction variants. While ensemble median CE is mostly negative, for iterations that use early calibration periods (1884–1954, 1889–1959, and 1894–1964) positive CE scores are observed from approximately 1650 to the present. The best reconstruction has an early calibration period (1884–1954), excludes the Sr/Ca record from Tonga [*Wu et al.*, 2013], and is most robust (positive RE and CE) from 1649 to 1999. Due to low CE, trends and decadal variability prior to 1649 and after 1999 should be interpreted with caution.

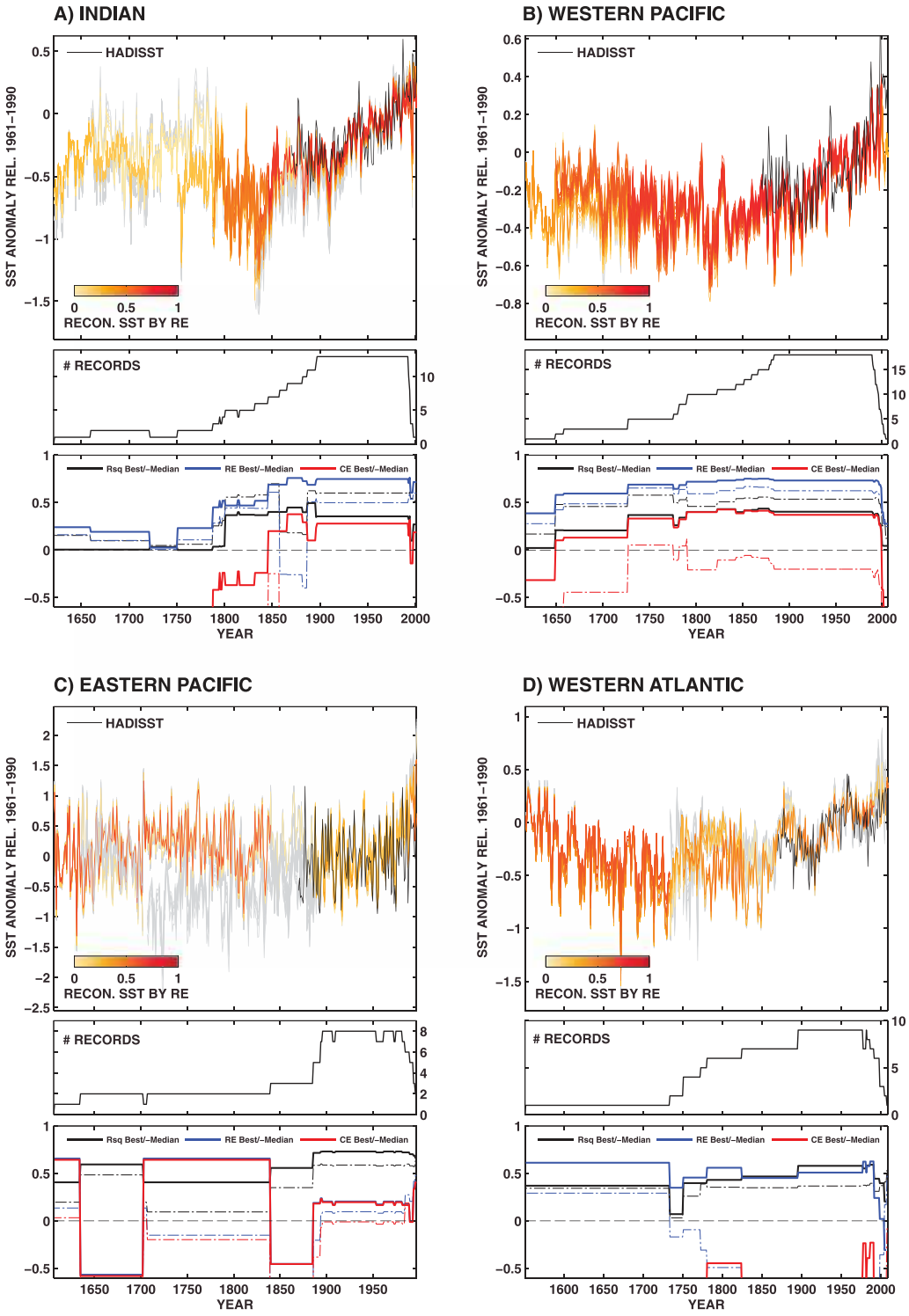

Figure 2. (a–d) The four regional CPS SST reconstructions. For each region, (top) the ensemble of reconstructed SSTs created by systematically leaving one proxy out and changing the calibration and validation periods is shown. The ensembles are color coded by the reduction of error statistic (RE). Higher RE (in red) indicates better skill. The black line indicates instrumental (HadISST) SSTs for the target regions. (middle) The number of paleoclimate records available through time; (bottom) the validation statistics associated with the best reconstruction (solid lines) and the median values for the ensemble of reconstructions (dotted lines).

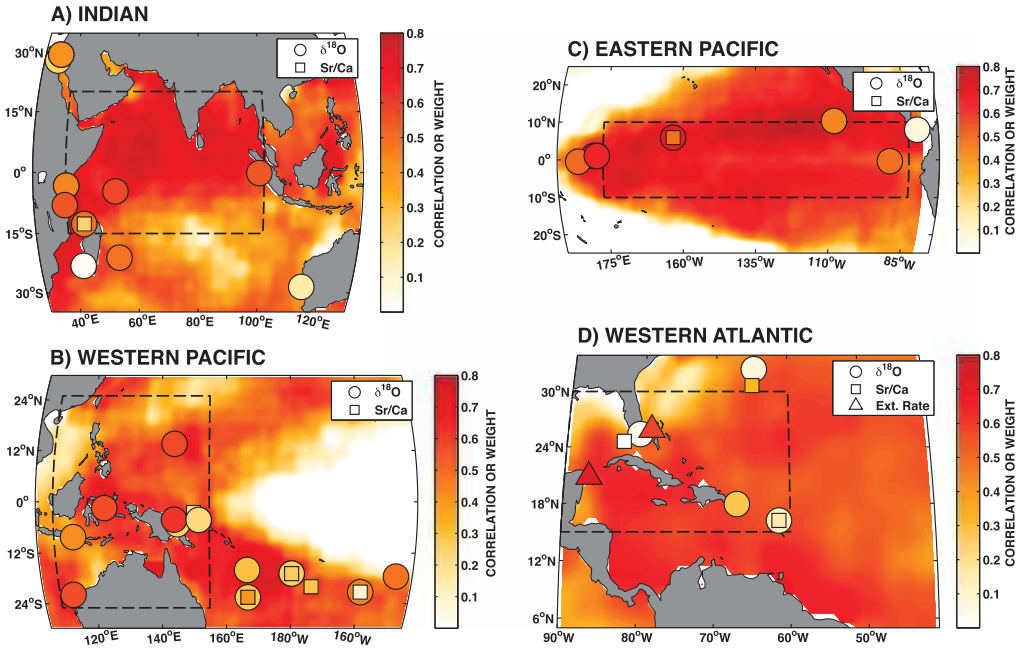

Figure 3. (a–d) Field correlations and record contributions to the regional reconstructions. For each region, the dots represent the location of the coral records and their contribution to the reconstruction, as represented by their $r(1 - p)$ weight (see description in main text). The background colors represent the field correlation (r) between the best reconstruction for each basin and HadISST over the instrumental period. The dotted rectangles outline the target regions.

Coral records from throughout the central warm pool and South Pacific region contribute equally to the western Pacific reconstruction (Figure 3b), and a field correlation using the best reconstruction produces a horseshoe-shaped pattern of coherent SST variability that extends out from the western equatorial Pacific into the subtropics in both hemispheres (Figure 3b). The coral records from the South Pacific, which consist of Sr/Ca and δ^{18}O data from Fiji [*Bagnato et al.*, 2005; *Linsley et al.*, 2006], Rarotonga [*Linsley et al.*, 2006], Vanuatu [*Quinn et al.*, 1996; *Gorman et al.*, 2012], New Caledonia [*Quinn et al.*, 1998; *DeLong et al.*, 2012, 2013], and Tonga [*Wu et al.*, 2013] include the longest records in the western Pacific collection, and prior to 1782 the reconstruction is based solely on data from these sites. Because of this, variability in the western Pacific SST reconstruction prior to 1782 may be biased toward the South Pacific and may not accurately reflect the SST target if SST and/or seawater δ^{18}O variations in the South Pacific were not teleconnected with the western Pacific as in the calibration period. The coolest decade in the best reconstruction of western Pacific SSTs was 1808–1817 (-0.5°C), and the ensemble members demonstrate that this feature is not clearly attributable to a single record (Figure 2b). The warmest decade of the reconstruction is 1987–1996 (0.1°C).

3.3. Eastern Pacific

The eastern Pacific reconstruction is based on up to eight records and spans the period from 1607 to 1998 (Figure 2c). Eighty-one percent of the eastern Pacific SST ensemble reconstruction members have a median RE and CE throughout the last 400 years that is below zero, indicating that the composite of the paleoclimate data in this region generally produces reconstructions without skill. There are, however, 12 reconstruction realizations with positive RE and CE. Of these, the iterations with median RE and CE substantially above zero (>0.02) exclude either the Palmyra Island [*Cobb et al.*, 2003] or Secas Island [*Linsley et al.*, 1994] δ^{18}O time series. Not surprisingly, the Secas Island δ^{18}O record, interpreted as an indicator of seawater δ^{18}O anomalies associated with regional Intertropical Convergence Zone position [*Linsley et al.*, 1994], has a very low correlation with target SST ($r = -0.10, p = 0.34$, Table 1)—hence, its exclusion increases the skill of the reconstruction. Palmyra Island δ^{18}O has a significant and high correlation with target SST ($r = -0.71, p < 0.001$, Table 1) but contributes to poor validation RE and CE values because it has a strong secular trend in δ^{18}O from ~1970 to 1998 that is not reflected in the instrumental target SSTs [*Cobb et al.*, 2003; *Nurhati et al.*, 2009]. The origin and interpretation of this trend, seen in many central equatorial Pacific δ^{18}O records, are discussed further in section 4.3.

The best reconstruction excludes Secas Island $\delta^{18}O$, has an early calibration period (1897–1953), and is most robust from 1607 to 1634, 1703 to 1839, and 1886 to 1998. The intervals from 1635 to 1702 and 1840 to 1885 have negative RE and CE and should not be interpreted. The field correlation map indicates that the best eastern Pacific reconstruction captures SST variability throughout the eastern and central Pacific (Figure 3c). The coldest decade in the best reconstruction (spanning 1607–1997) is 1805–1814 (−0.4°C), and the warmest decade is 1985–1994 (0.8°C).

3.4. Western Atlantic

The western Atlantic reconstruction consists of up to nine records and spans the period from 1552 to 2009 (Figure 2d). For 91% of reconstruction ensemble members, median RE and CE are negative from 1734 to 2009, indicating that when the proxy data are composited they produce a reconstruction without skill. Prior to 1734, the reconstruction is based on a single coral extension rate data set from the Bahamas [*Saenger et al.*, 2009] that calibrates and validates such that RE is positive for this single-record nest 74% of the time. There are only a few (4/70) iterations where RE is positive during the instrumental period; these iterations, which include the best reconstruction, exclude the extension rate data from the Yucatan [*Vásquez-Bedoya et al.*, 2012]. The best reconstruction has a late calibration period (1930–1988), with positive RE from 1552 to 2004. However, as CE is still negative for this reconstruction, low-frequency variance must be interpreted cautiously.

The extension rate data from the Bahamas [*Saenger et al.*, 2009] and the Yucatan [*Vásquez-Bedoya et al.*, 2012] have the highest weights in the reconstruction (0.58 and 0.72, respectively; Figure 3d) because they exhibit strong multidecadal variability that closely matches the instrumental record of regional SSTs. The Yucatan data, however, do not validate (RE and CE) over the most recent two decades (1990–2008) and hence contribute to lower validation statistics when included in the composite. Data from the Dry Tortugas and the Florida Straits contribute minimally to the regional reconstruction, possibly because SST variability is highly dynamic in this region and not well correlated with central and southern Caribbean SSTs [*DeLong et al.*, 2014]]. Although the western Atlantic proxy collection is limited in its spatial extent and has relatively low skill, a field correlation between reconstructed and observed SSTs during the instrumental period indicates that the reconstruction captures SST variability typical of the greater tropical Atlantic region (Figure 3d). The warmest decade of the best reconstruction (spanning 1552–2007) is 1995–2004 (0.4°C), and the coolest decade is 1825–1834 (−0.7°C).

3.5. Region Summary

Figure 4 shows the best reconstructions from each basin and their validation RMSE estimates. All reconstructions show warming in the middle to late nineteenth and twentieth centuries, although validation statistics suggest that the trends in the western Atlantic in particular should be interpreted cautiously. Furthermore, the reconstructed warming in the eastern Pacific region does not agree with instrumental observations (see discussion in section 4.3 below). The western Pacific region displays the smallest SST range, with SSTs changing less than a degree during the last four centuries. The Indian and western Atlantic reconstructions display a slightly greater range (approximately 1.5°C), and the eastern Pacific reconstruction exhibits a much larger SST range (approximately 2°C); these results are consistent with historically observed differences in SST variations in the four basins.

3.6. Sensitivity Tests

As described in section 2.2, we tested the sensitivity of our results to our choice of instrumental SST product by repeating the analyses using the ERSST v3b data set [*Smith et al.*, 2008]. For all basins, we found that the best reconstructions were very similar ($r > 0.99, p \ll 0.001$) with the primary difference being the amplitude of the reconstructed trends (Figure 5). The mean amplitudes of the ERSST v3b-derived reconstructions were larger than those in the HadISST reconstructions for the Indian and western Pacific regions, by 38% and 25%, respectively (Figure 5). This is not unexpected, as ERSST v3b generally exhibits stronger recent warming trends than the HadISST product [*Emile-Geay et al.*, 2013a]. In the western Atlantic and eastern Pacific regions, where multidecadal and interannual variability dominate the instrumental record, respectively, the amplitudes of the ERSST v3b reconstructions are comparable to the HadISST reconstructions (4% difference for the western Atlantic and 6% difference for the eastern Pacific). We conclude from this experiment that the choice of instrumental SST product has little impact on the resulting reconstructions beyond affecting the magnitude of long-term trends, which scale in relation to the trends evident in the respective instrumental data sets.

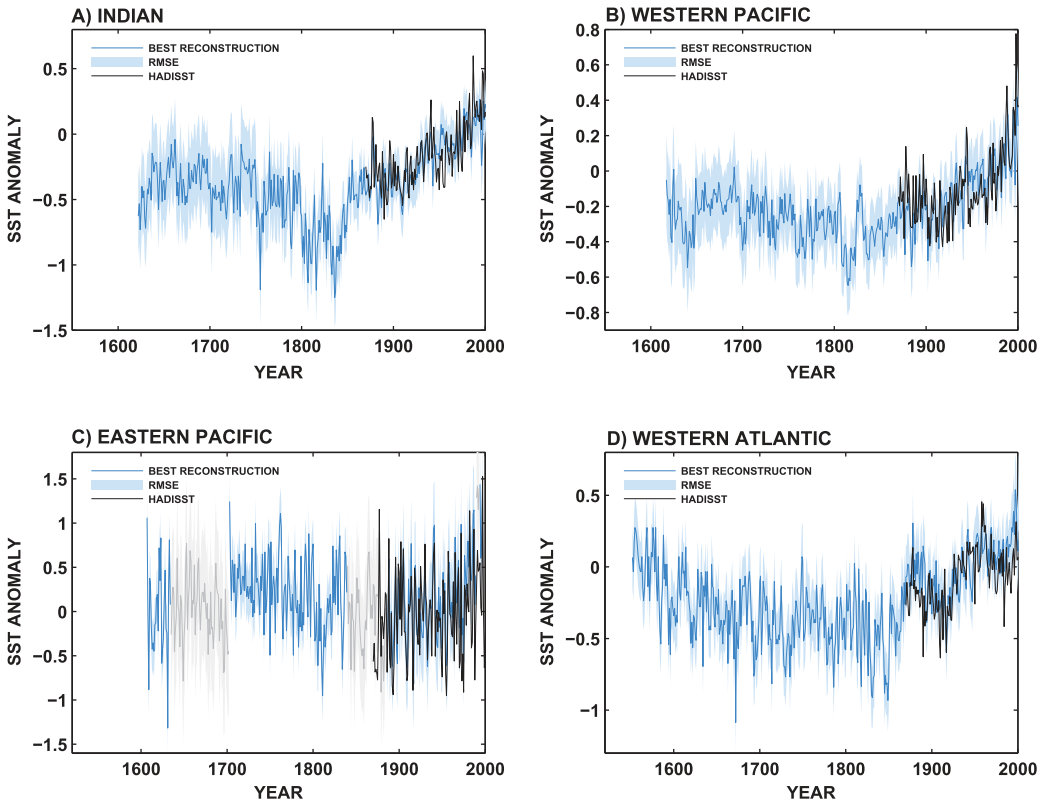

Figure 4. (a–d) The best (highest cumulative RE) reconstruction for each of the four target regions, with root-mean-square errors (RMSEs) and instrumental HadISST (in black). Portions of the reconstruction where RE ≤ 0 are plotted in gray.

We also tested the sensitivity of our reconstructions to our weighting scheme (section 2.4). In our standard methodology, the contribution of each proxy time series to the composite is weighted by its correlation to the target SST, adjusted by the significance of the correlation ($r(1 - p)$, section 2.4). Results using no weighting ($r^0(1 - p)$) and a stronger weighting ($r^2(1 - p)$) are very similar, with minor differences emerging under the "no weighting" scenario in the Indian and western Pacific reconstructions (Figure 5). We note that the results employing no weighting still exclude those records with zero or physically implausible correlations (section 2.4), which amounts to four records in the western Atlantic and five records in the western Pacific (Table 1). The low sensitivity to weighting scheme is expected, given that the correlations with target SST are relatively high for most of the data series (Table 1) and the mechanisms linking them to SSTs are well understood. We conclude that our choice of proxy-weighting method has little impact on the reconstruction results.

4. Discussion

4.1. Reconstruction and Data Uncertainties

In determining which features of our reconstruction are robust, a number of uncertainties must be considered. These uncertainties arise from (1) limited observations in time and space (Figure 1 and Table 1); (2) imperfect mapping of the paleoclimate data to the target variable and region (Figures 1–3), including knowledge that variance in proxy measurements may depend on the $\delta^{18}O$ of seawater, temperature, seasonal changes in growth rate, and biological factors; (3) choice of reconstruction weighting scheme (Figure 5); and (4) choice of historical product for SST target (Figure 5). Our algorithm, in common with most approaches to paleoclimate reconstruction, also assumes that the correlation between each time series and variance within the target region is time stationary. In this case, we find that neither the weighting scheme nor target SST has a large influence on our reconstructions. Rather, the primary sources of uncertainty and reduction of validation skill are those associated with the inclusion or exclusion of particular data sets and the potential nontemperature and multivariate influences on individual proxy records. An advance in this

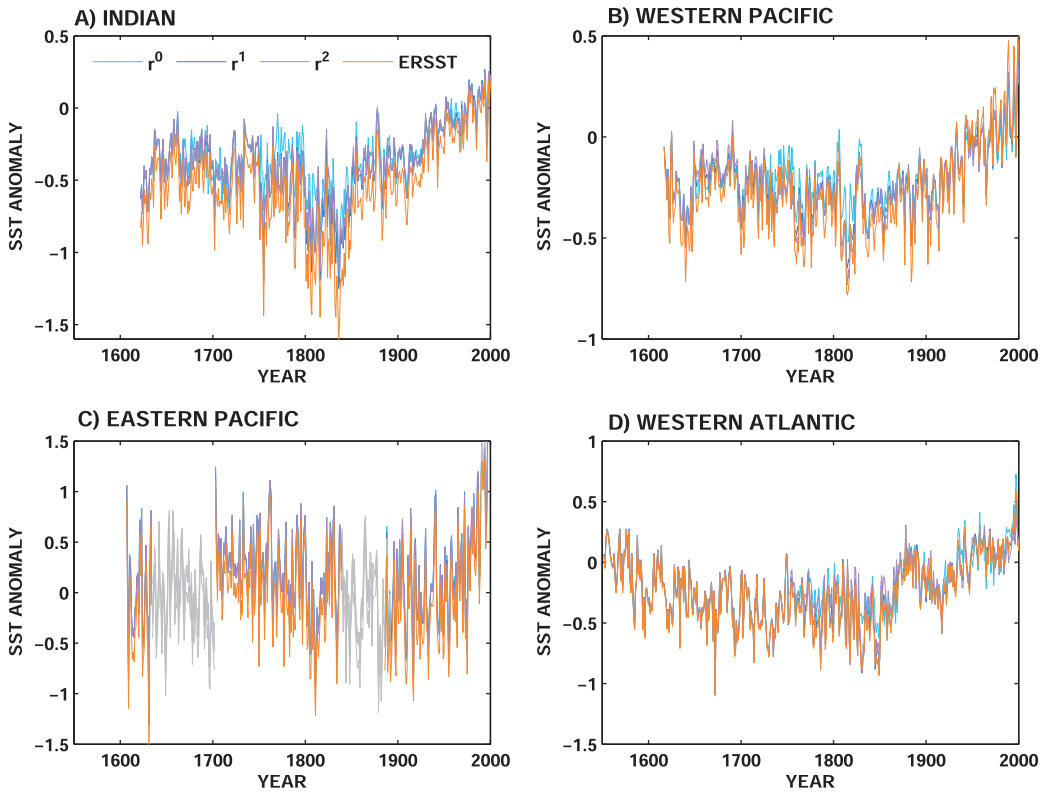

Figure 5. (a–d) The effect on the reconstructions of changing the target SST data set and weighting scheme. Blue to purple lines show the best reconstructions for each of the target regions using no weighting (r^0), our standard weighting (r^1), and heavier weighting (r^2). The orange line shows the best reconstruction for each region when using the ERSST v3b instrumental product rather than HadISST. Portions of the reconstruction where RE $\leq$ 0 are plotted in gray.

work is the use of more sampling and detection of these uncertainties. In particular, "forward" validation against the most recent regional SST observations shows that several proxies with significant correlations to the target field in earlier epochs overestimate modern trends in the eastern Pacific and western Atlantic for the last several decades, which results in reduced skill and poor validation. Despite these uncertainties and varying levels of skill, the temporal evolution of the Indian, western Pacific, and western Atlantic targets are very similar across ensemble members (intraensemble mean correlations: Indian $\bar{r} = 0.94 \pm 0.06$, range = 0.67 to 1.0; western Pacific $\bar{r} = 0.98 \pm 0.03$, range = 0.80 to 1.0; western Atlantic $\bar{r} = 0.94 \pm 0.08$, range = 0.62 to 1.0), while the eastern Pacific ($\bar{r} = 0.87 \pm 0.21$, range = 0.29 to 1.0) shows greater transient dependency on proxies and calibration periods (Figure 2). These intraensemble mean correlation values are, however, inflated by the nonunique subsets of paleoclimate data used across the different members.

4.2. Mean Spectral Characteristics of Tropical SSTs

Coupled climate modes such as ENSO and the Atlantic Multidecadal Oscillation (AMO) exert substantial influence on SST variability in the tropics. Our coral-based reconstructions provide a composite historical perspective on how these coupled modes may have changed through time. Comparison in the frequency domain between our reconstructions and observational SSTs over the time span of the observational period (1870 to present) demonstrates that our reconstructions capture the spectral characteristics of modern tropical ocean SST variability in our Indian, western Pacific, and Atlantic regions, including interannual spectral peaks associated with ENSO and multidecadal power associated with the AMO (blue lines, Figure 6). The exception is the presence of low-frequency power in our eastern Pacific reconstruction, which we believe is a reflection of a spurious reconstructed warming trend, as discussed further below.

The spectra of the full reconstructions for each basin indicate that interannual variability similar to the observations is generally persistent throughout the span of the reconstruction (black and gray lines, Figure 6). Multidecadal power is also comparable to that seen in the observational record, and there are

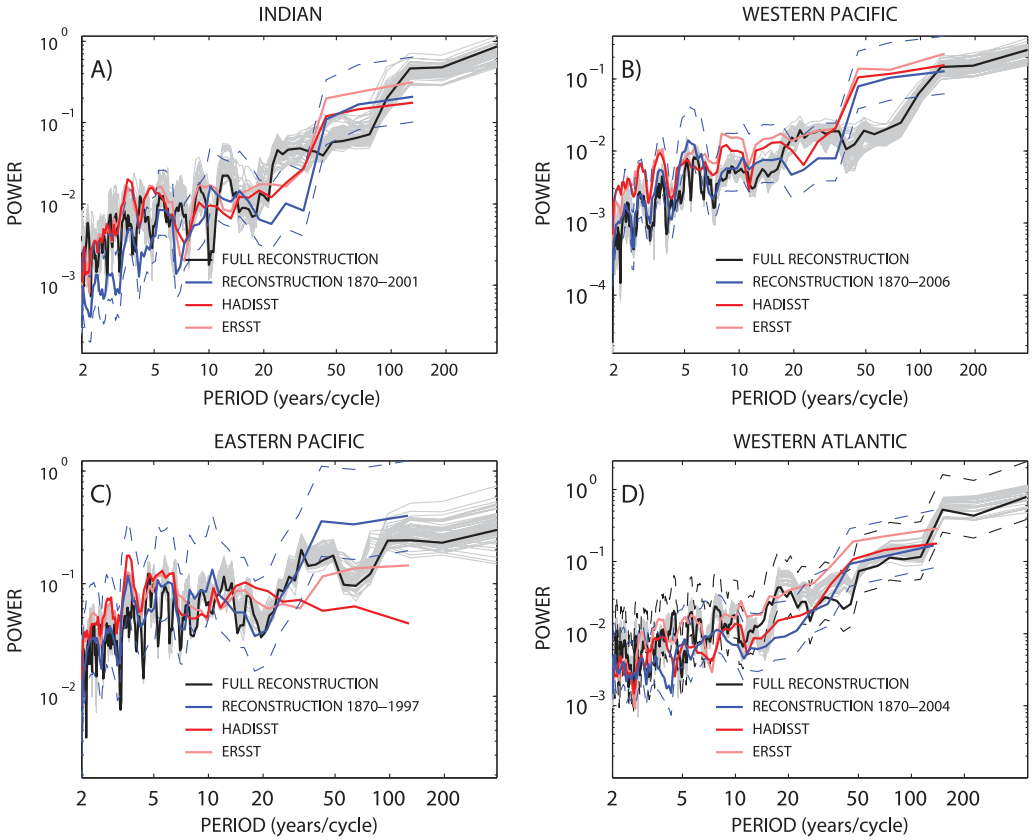

Figure 6. (a–d) Multitaper spectra comparison for the four basin reconstructions and observations, over the instrumental period and over their respective full periods. The best reconstruction over the full time period from each basin is plotted in black, and reconstruction ensemble members are shown in gray. The blue line indicates the best reconstruction over the instrumental time period alone, and dashed blue lines indicate the 95% confidence interval. Darker red lines denote the corresponding spectral density estimation of the HadISST observations from each basin; light red lines denote the spectral density estimation of the ERSST v3b observations.

few spectral estimates that are not consistent within uncertainty. The Atlantic reconstruction, however, suggests an additional spectral peak with a 20 year periodicity not seen in the observational era (Figure 6d). This frequency of SST variability is a prominent feature of the coral extension rate record from the Bahamas [*Saenger et al.*, 2009], which is the sole coral record comprising the reconstruction prior to 1734. This frequency may represent an interdecadal mode of Atlantic SST variability that is overprinted during the observational period by the 70 year (AMO-type) structure [*Saenger et al.*, 2009] or otherwise not well captured in the short span of the observational data set. It may also simply be a characteristic unique to this single record.

4.2.1. Transient Spectral Characteristics of Tropical SSTs

To investigate the spectral evolution of SST variability over time, we applied an evolutive spectral analysis to each of the best reconstructions (Figure 7). We also band-pass filtered the best reconstructions over key frequencies to illustrate and analyze interannual variability associated with ENSO (3–7 year; Figure 8) and multidecadal variability (20–80 year; Figure 9).

4.2.1.1. Interannual Variability

The 3–7 year band-passed western Pacific and eastern Pacific reconstructions are strongly and significantly correlated with 3–7 year band-passed annual April–March NINO 3.4 SST with the expected sign ($r = -0.84$ and $r = 0.90$, respectively; $p \ll 0.001$ in both cases, accounting for effective degrees of freedom) suggesting that power in this frequency band is closely associated with ENSO (Figure 8). The band-passed Indian reconstruction is also correlated with NINO 3.4 with the expected sign, but weakly so ($r = 0.32$, $p = 0.04$), possibly reflecting the influence of shorter-timescale climate phenomena, such as positive IOD events, that are not

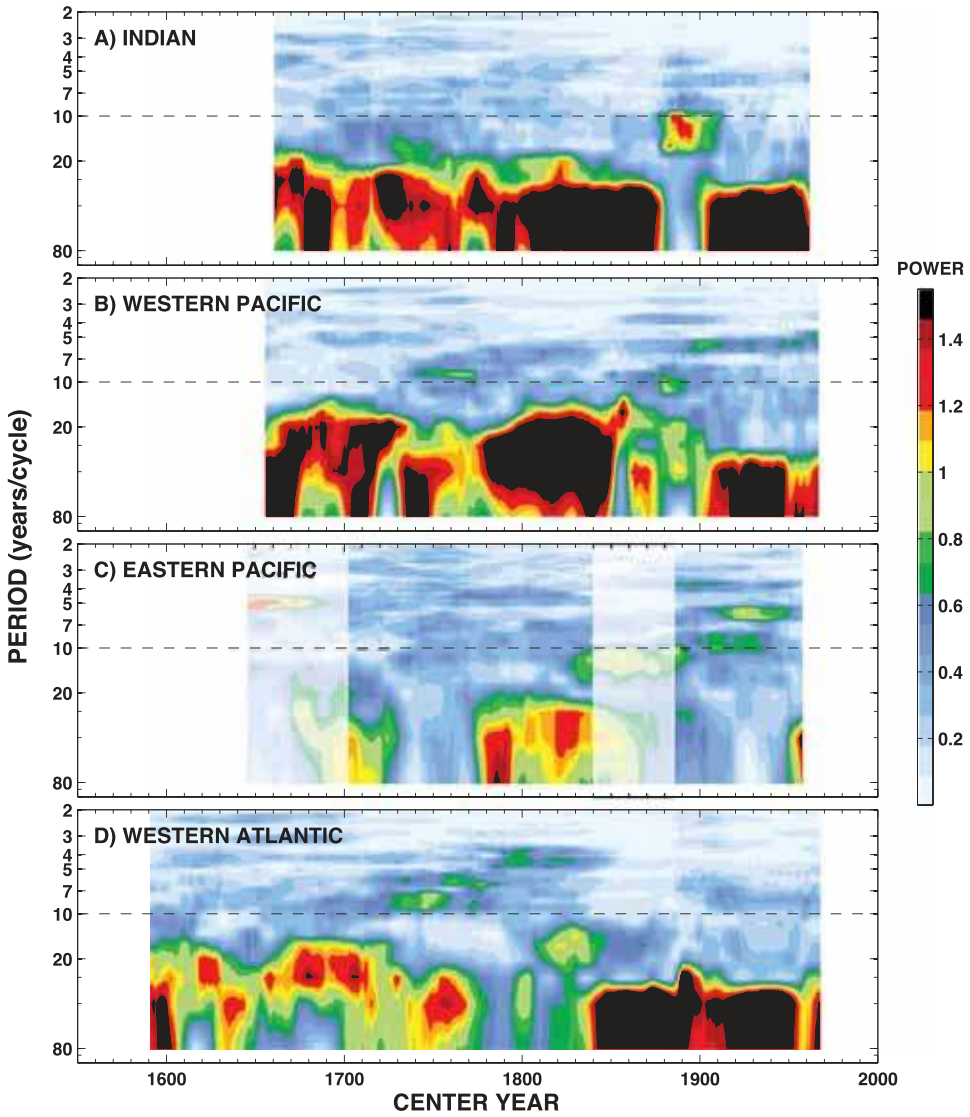

Figure 7. (a–d) Evolutive (50 year window) multitaper method spectra of the best reconstructions for each basin. Portions of the reconstruction where RE ≤ 0 are shaded in white. The black dashed horizontal line in each panel indicates the 10 year periodicity.

always concurrent with ENSO events. The band-passed Atlantic reconstruction has a similarly weak correlation with NINO 3.4 ($r = 0.34$, $p = 0.01$), potentially reflecting the teleconnected influence of ENSO on trade wind intensity and latent heat flux in the tropical Atlantic Ocean [*Enfield and Mayer*, 1997].

Both the eastern and western Pacific reconstructions show active ENSO variability (defined as amplitude in excess of 1.5 standard deviations) in the late nineteenth and twentieth centuries (Figures 7, and 8b, and 8c) in agreement with instrumental observations of ENSO (Figure 8e). The western Pacific reconstruction also indicates active ENSO variability from circa 1920 to 1940, which differs slightly from the NINO 3.4 observations (Figure 8). Given limited observations of central Pacific SSTs in the early twentieth century, it is difficult to assess whether the disagreement is attributable to uncertainties in the observations or in the coral-based reconstruction, respectively. Moving back in time, the western and eastern Pacific reconstructions differ enough such that the correlation between the band-passed records is significant but relatively low ($r = -0.45$, $p \ll 0.001$). This may be due in part to the limited skill of the eastern Pacific reconstruction (Figure 2c). Thus, the western Pacific reconstruction, which has the most consistently reliable skill (Figure 2b), gives us the most robust and continuous window into interannual SST variability associated with ENSO

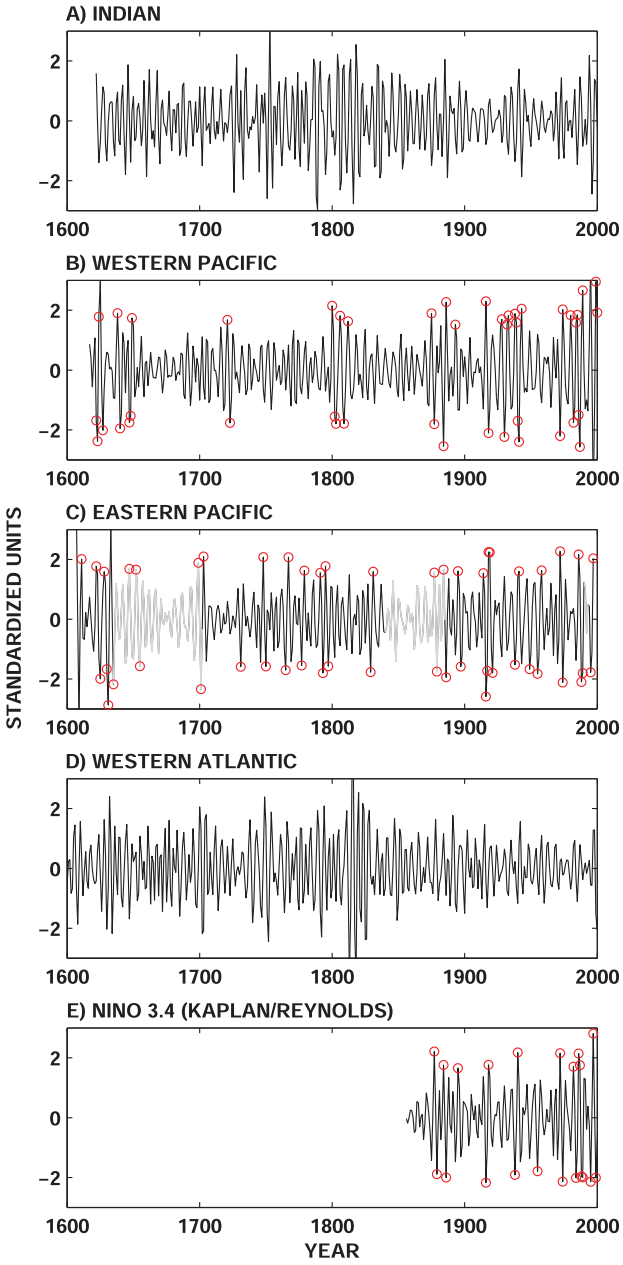

Figure 8. SST variability in the ENSO (3–7 year) band in all (a–d) four reconstructions, with (e) instrumental SST variability in the NINO 3.4 region shown for comparison [*Reynolds and Smith*, 1994; *Kaplan et al.*, 1998]. Red circles denote times when variance in this bandwidth exceeded 1.5 standard deviations in the western Pacific, eastern Pacific, and NINO 3.4 regions and may be interpreted as "active ENSO periods." In all cases, we applied a 3–7 year seven-point Butterworth band-pass filter to isolate ENSO variability. The portions of the reconstructions that have an RE value equal to or below zero are plotted in gray.

periodicities. The filtered time series and evolutive spectra from the western Pacific reconstruction suggest that ENSO has varied persistently across the past four centuries (Figures 7 and 8). The variance of the data in the 3–7 year band is significantly higher ($p = 0.02$, Shoemaker's F test [*Shoemaker*, 2003], evaluated against a 3–7 year band-passed red noise null) in the industrial period (1850 to present, mean variance = 1.46σ) compared with the rest of the record (1617–1850, mean variance = 0.72σ), but the variance in the early seventeenth century (1617–1660; 1.39σ) is comparable ($p = 0.96$).

Though limited in skill, the eastern Pacific reconstruction also suggests comparable ENSO variance in the seventeenth century and the twentieth century, as do previous studies of ENSO-sensitive coral records in the central Pacific [*Cobb et al.*, 2003]. Thus, we find no consistent evidence in our reconstructions for an anthropogenically forced change in the magnitude of interannual SST variability across the tropical Pacific Ocean. Long control simulations conducted with coupled climate models likewise show that the modulation of ENSO power is a feature that emerges naturally from the climate system and need not be externally forced [*Wittenberg*, 2009]. An additional caveat to our analysis, however, is the fact that small age uncertainties in individual coral records (on the order of several years) averaged within our reconstruction methodology can reduce the spectral power in the interannual band and therefore result in underestimation of ENSO power in the past [*Comboul et al.*, 2014].

4.2.1.2. Multidecadal Variability

Multidecadal power in the Indian Ocean, and potentially the western Pacific reconstructions, appears reduced in the twentieth century relative to previous centuries (Figures 7 and 9), in agreement with a previous analysis of coral $\delta^{18}O$ data across the Indo-Pacific [*Ault et al.*, 2009], but these differences are not significant when tested against a filtered, red noise null. There is also a tendency toward higher multidecadal variance in the Indian, western Pacific, and eastern Pacific reconstructions during the early nineteenth century, though it is not significantly different from multidecadal variance in the rest of the records at the 5% level. Our observation

of possibly higher multidecadal variability during the early 1800s is consistent with a tree ring- and coral-based warm pool SST reconstruction [*D'Arrigo et al.*, 2006] as well as individual warm pool coral records [*Osborne et al.*, 2014].

The Atlantic reconstruction shows persistent multidecadal variability, but power in the ~70 year AMO band appears to vary throughout the record (Figures 7 and 9) and is weaker in our reconstruction prior to ~1840. There is also substantial interdecadal (~10 to 50 year) power before the onset of the modern observational era. Given the limited skill of the western Atlantic reconstruction (see section 3.4 and Figure 2d), however, and the fact that it is only based on one proxy record prior to 1734, it is not possible to determine whether this suggests that AMO band (70 year) multidecadal power was smaller in the past. While some of the observed multidecadal Atlantic SST variability may reflect the influence of the large-scale global temperature signal projected on the northern Atlantic region [*Mann and Emanuel*, 2006], other proxy-based reconstructions suggest that multidecadal variability is a persistent feature of the Atlantic [*Gray et al.*, 2004; *Shanahan et al.*, 2009; *Svendsen et al.*, 2014; *Kilbourne et al.*, 2014] at least over the last several centuries. The tree ring-based AMO reconstruction from *Gray et al.* [2004] shows a similar eighteenth century loss of decadal and bidecadal power seen in our spectral analysis (Figure 7), suggesting this could be a robust feature of North Atlantic climate history. Model simulations also suggest a persistent although variable and quasiperiodic ~55 to 80 year cycle throughout the last millennium and the Holocene [*Landrum et al.*, 2013; *Wei and Lohmann*, 2012], and Atlantic multidecadal variability is reproduced in long unforced global climate model control simulations [*Knight et al.*, 2005]. However, the lack of skill throughout much of our Atlantic reconstruction and the limits this places on interpretability clearly indicates that more long, coral-based records from the Atlantic region are needed to assess whether AMO variability has persisted in the past.

4.3. Secular Trends

SiZer analyses indicate that the reconstructions of the Indian and western Pacific regions show similar long-term temperature trends (Figures 10a and 10b). Though validation CE is low for the Indian reconstruction prior to 1840, it shows a cooling from approximately 1700–1820 in agreement with the western Pacific. This cooling is then followed by a robust warming trend through the present in both regions (Figures 10a and 10b). This suggests a generally similar evolution of SSTs across the Indo-Pacific warm pool since the eighteenth century, although according to the best reconstructions, the Indian Ocean was cooler during the early nineteenth century (on average, −0.8°C below 1961–1990 mean) than the western Pacific (on average, −0.4°C below 1961–1990 mean). In addition, the rate of the modern warming is slightly larger in the Indian Ocean (since 1850, 0.040 ± 0.004°C, 95% confidence interval (CI), per decade) than in the western Pacific (0.031 ± 0.004°C per decade). This difference may be attributable to the limits that deep convection and evaporative cooling imposes on the rates of warming in the warm pool region [*An et al.*, 2012].

Both the magnitude and shape of the long-term trends in the Indian and western Pacific Ocean reconstructions are in general agreement with previous reconstructions of Indo-Pacific SSTs [*D'Arrigo et al.*, 2006; *Wilson et al.*, 2006], which is expected because these reconstructions contain many of the same coral data series used here. Our reconstructions agree in sign but disagree in timing and amplitude with sediment foraminiferal Mg-/Ca-based estimates of western Pacific warm pool SSTs [*Oppo et al.*, 2009]. The latter suggests that the 1700s, not the 1800s, contained the coolest temperatures of the last 400 years and that the warm pool has warmed by 1.7°C since 1850, rather than by 0.5°C as our reconstructions suggest. Our choice of SST product cannot explain this discrepancy, as the inferred warming since 1850 using the ERSST v3b product for calibration is only slightly larger (0.6°C). The Mg/Ca sedimentary record, however, is subject to uncertainties in dating as well as in the calibration of foraminiferal Mg/Ca [*Oppo et al.*, 2009]. Our western Pacific and Indian reconstructions show good agreement with instrumental trends (Figures 2a and 2b), giving us confidence in the magnitude of the reconstructed changes.

The western Atlantic has a generally similar SST evolution to that of the Indo-Pacific warm pool. Although the initial significant cooling appears to end earlier (circa 1700) (Figure 10d), low CE values for even the best reconstruction limit a robust determination of whether this difference is significant. The modern warming trend begins in the early 1800s, in general agreement with the tropical Indo-Pacific regions. The overall average rate of warming in the western Atlantic since 1850 (0.037 ± 0.006°C per decade; note that the result using ERSST v3b is identical at 0.039°C per decade) is similar to that in the Indian and western Pacific. The magnitude of warming since 1850 implied by this rate (0.6°C) is similar to the magnitude of SST change

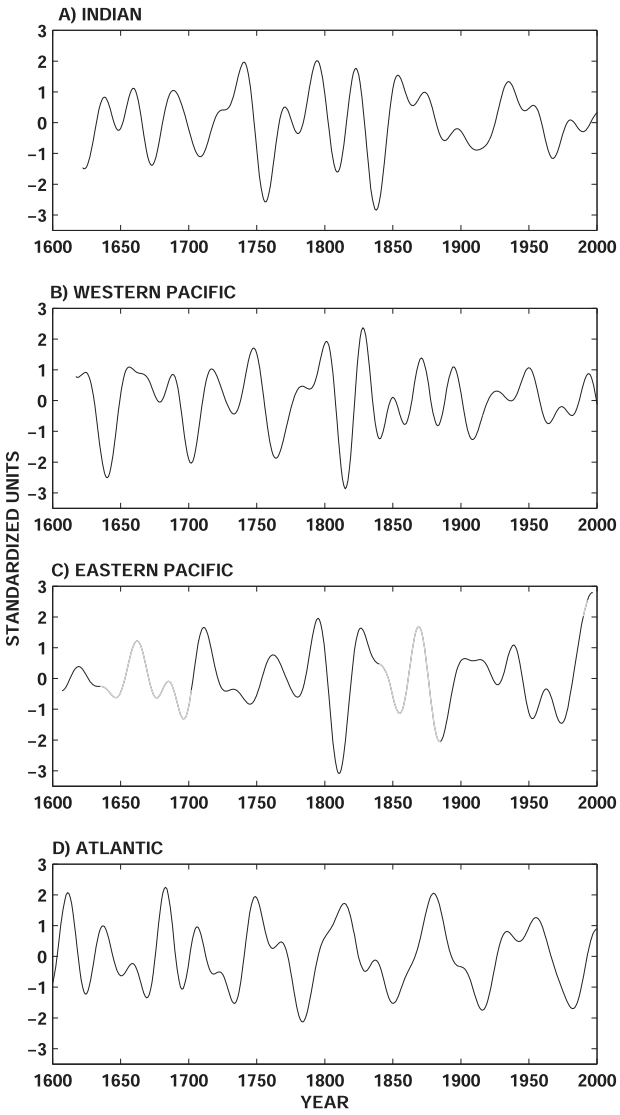

Figure 9. (a–d) SST variability in the multidecadal (20–80 year) band in all four reconstructions, isolated with a 20–80 year seven-point Butterworth band-pass filter. The portions of the reconstructions that have an RE value equal to or below zero are plotted in gray.

independently estimated from a sediment foraminiferal Mg/Ca reconstruction from the Cariaco Basin [*Black et al.*, 2007], but about half as much as the magnitude of warming independently estimated from a sediment foraminiferal Mg/Ca reconstruction from the Gulf of Mexico (approximately 1.5°C [*Richey et al.*, 2007, 2009]). Notably, *Black et al.* [2007] calibrated their Mg/Ca data directly to instrumental SST, resulting in a Mg/Ca sensitivity to temperature that is nearly twice as high (17%) as the 9% value typically seen in culture and sediment trap calibrations [*Lea et al.*, 1999; *Anand et al.*, 2003]. The result is a SST reconstruction with about half the amplitude typical of Mg-/Ca-based reconstructions, but in better agreement with the instrumental trends and our coral-based reconstruction.

The best eastern Pacific reconstruction suggests that the region has been warming at a rate of 0.095 ± 0.03 (95% CI)°C per decade from 1900 to 1998. This is higher than the rate implied by the ERSSTv3b product (0.06°C per decade, $p = 0.0009$, Mann-Kendall test) and much higher than the rates associated with the nonsignificant warming trends in HadISST (0.02°C per decade, $p = 0.34$) and the HadSST3 product (0.04°C per decade, $p = 0.15$). Closer inspection reveals that while the reconstruction captures the interannual variability in eastern Pacific SSTs well, reconstructed temperatures begin to rise above observed values in the 1970s (Figure 11). Seven of eight records that comprise the eastern Pacific reconstruction consist of $\delta^{18}O$ data; thus, their composite may reflect changes in the $\delta^{18}O$ composition of seawater in addition to temperature (section 1). On interannual timescales, regional changes in $\delta^{18}O$ and SST act in concert in the closely coupled ocean and atmosphere of the eastern Pacific to raise or lower coral $\delta^{18}O$ [c.f. *Evans et al.*, 2000; *Cobb et al.*, 2003; *Nurhati et al.*, 2011]; That is, a regional warming during an El Niño event is usually accompanied by increased rainfall, both of which decrease $\delta^{18}O$ in coral aragonite. The existence of a strong apparent "warming" trend in the eastern Pacific reconstruction since 1960 may therefore represent a secular shift in seawater $\delta^{18}O$ values that is not proportional to the interannual coupling between temperature and seawater $\delta^{18}O$. A pronounced negative $\delta^{18}O$ trend is most prominent in the central Pacific corals from Palmyra, Maiana, and Tarawa Atolls, all of which are used in the eastern Pacific reconstruction (Figure 11). The trend is less apparent in $\delta^{18}O$ data from modern coral specimens from Christmas and Fanning Islands (Figure 11), but these data sets are not long enough to be included in our eastern Pacific compilation. Notably, the Sr/Ca data from Palmyra do not show a warming trend ($p = 0.30$, Figure 11), and neither do the $\delta^{18}O$ data from the Galapagos Islands ($p = 0.12$ [*Dunbar et al.*, 1994]). These observations are consistent with

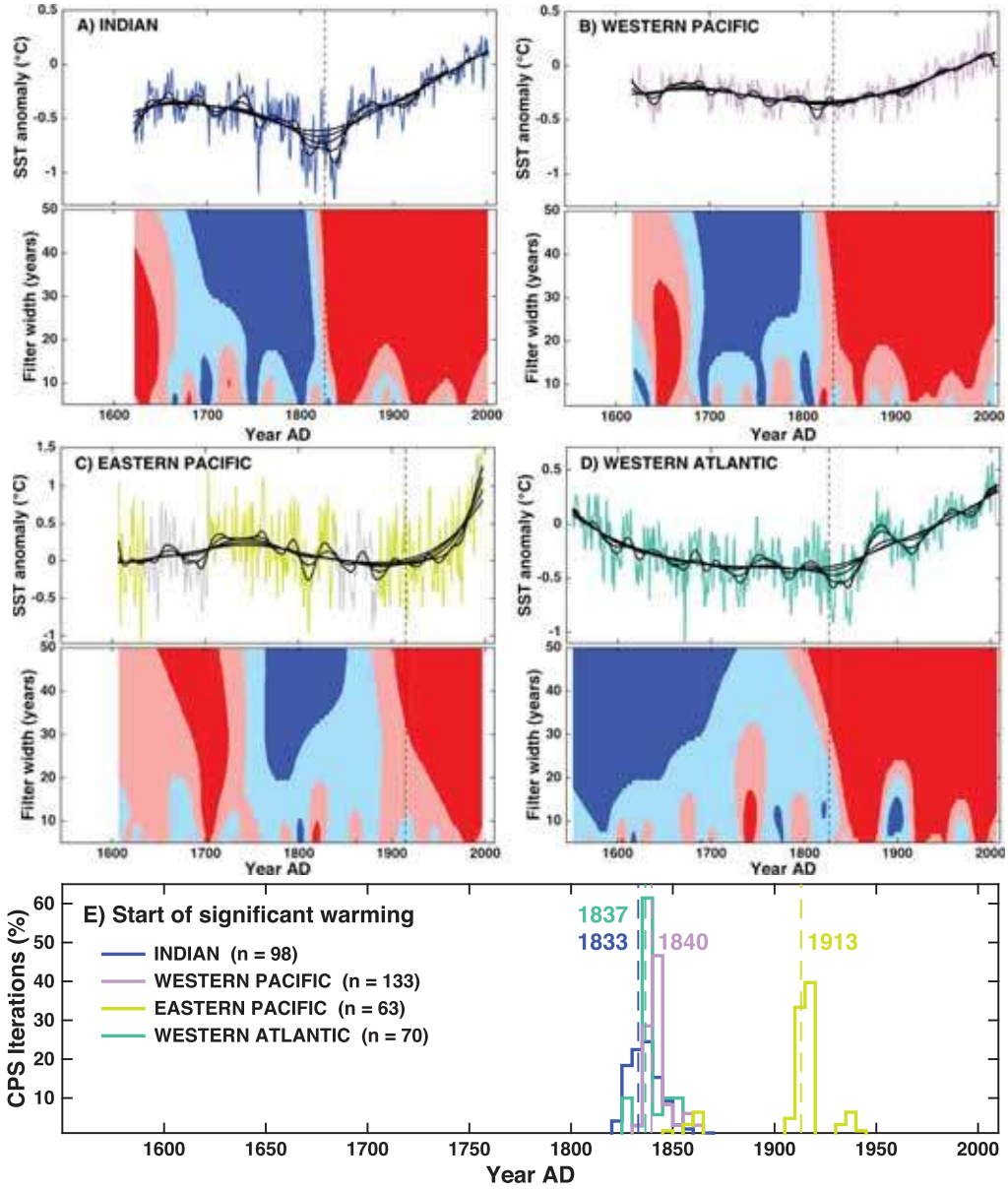

Figure 10. (a–d) SiZer analysis of the best reconstructions from each basin. (top) The annual reconstructions (colored; portions of the reconstruction where RE ≤ 0 plotted in gray) and a range of spline fits (in black; 5, 10, 20, 30, and 40 year filter widths). (bottom) The direction of the detected SST trends (blue = decreasing; red = increasing) and their significance (dark blue and red regions denote trends where $p < 0.1$) as a function of the width of the spline filter. Dashed vertical lines indicate the median timing of the onset of recent significant ($p < 0.1$) warming trends across 15–50 year filter widths. (e) SiZer-based histograms of the onset of recent significant warming. The histograms represent the median year across 15–50 year filter widths in which significant warming begins in all ensemble members for a given basin reconstruction. Vertical dashed lines and dates give the median change point across all ensemble members. For each reconstruction *n* denotes the number of ensemble members available.

the interpretation that the trend in $\delta^{18}O$ in the central Pacific corals reflects a change in the $\delta^{18}O$ of seawater in that region.

The cause of this secular $\delta^{18}O$ trend, which has been observed and documented previously [*Cole et al.*, 1993; *Cobb et al.*, 2001; *Evans et al.*, 1999; *Nurhati et al.*, 2009, 2011; *Kilbourne et al.*, 2004], is not completely understood. It is thought that the trend may reflect regional freshening [*Kilbourne et al.*, 2004; *Nurhati et al.*, 2011; *Thompson et al.*, 2011], possibly related to an anthropogenically driven thermodynamic enhancement

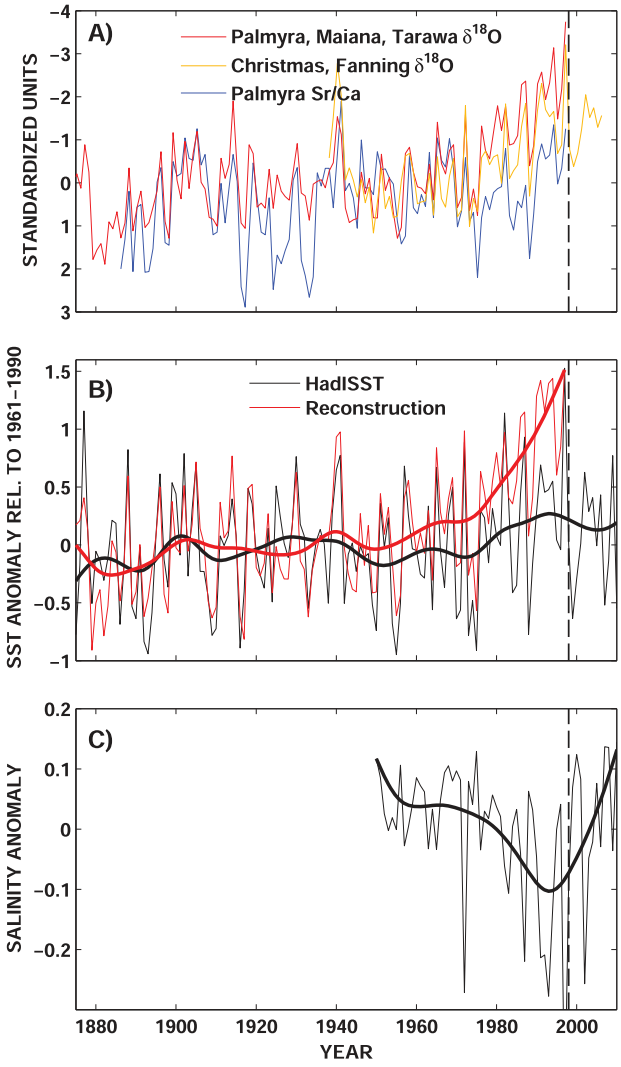

Figure 11. (a) Standardized δ^{18}O time series from central Pacific corals (in red: the average of data from Palmyra, Maiana, and Tarawa; in orange: the average of data from Christmas and Fanning Islands) show a strong negative trend since the midtwentieth century, whereas Sr/Ca data [*Nurhati et al.*, 2009] do not. Data are normalized to the 1940–1970 period for comparison. (b) Instrumental SSTs (HadISST, in black) do not show a strong warming trend, and our eastern Pacific reconstruction (in red) deviates from the instrumental data due to the influence of the trending δ^{18}O records. (c) Instrumental salinity data (UK Met Office EN3 data set) [*Ingleby and Huddleston*, 2007] from the central tropical Pacific (−5° to 5°N, 170°E to 150°W) show a freshening trend from 1950 to 2000, followed by a return to more saline conditions toward present. In all panels, thin lines represent annual data, and thick lines indicate 20 year Gaussian smoothed data. Dashed lines in each plot denote the year 1998, the end of the eastern Pacific reconstruction.

of the hydrological cycle [*Held and Soden*, 2006]. However, while salinity decreased in the central Pacific from 1970 to 2000 [*Morrissey and Graham*, 1996; *Delcroix et al.*, 2007; *Durack and Wijffels*, 2010], it has since increased again (Figure 11) [*Ingleby and Huddleston*, 2007], suggesting that the changes could also be linked to Pacific decadal variability [*Delcroix et al.*, 2007]. As our reconstruction ends in 1998, we cannot assess whether the corals would continue to predict anomalous "warming" due to more negative δ^{18}O values since 2000. However, coral data from Christmas and Fanning Islands do not show a trend in δ^{18}O between 2000 and 2007 (Figure 11) [*Cobb et al.*, 2013], suggesting that the central Pacific corals are continuing to follow the observed changes in salinity.

The three other regional reconstructions show a modern warming trend in qualitative agreement with observational data. The Indian, western Pacific, and Atlantic regions all show a coherent start to the modern warming trend during the early-to-middle 1800s (median values are 1833, 1840, and 1837 for the Indian, western Pacific, and Atlantic regions, respectively; Figure 10e). The delayed warming onset or absence of warming in the eastern Pacific during the twentieth century may result from the dynamic response of the coupled tropical Pacific Ocean-atmosphere to zonally uniform radiative forcing from greenhouse gases [*Clement et al.*, 1996; *Cane et al.*, 1997; *Solomon and Newman*, 2012], but currently, the lack of continuous, SST-sensitive coral data from the eastern and central Pacific prior to the twentieth century precludes an assessment of whether the recent observed changes are unusual in the context of past climate.

4.4. Relationships Between Tropical SSTs and Climate Forcings

Prior to the middle of the nineteenth century, the dominant radiative forcings on the climate system during the Common Era were volcanic and solar variability (Figure 12). Over this interval, and consistent with a recent and largely terrestrially derived composite analysis [*PAGES2k Consortium*, 2013], our reconstructions indicate that SST cooling was a feature of all of the tropical ocean regions with the possible exception of the eastern Pacific (Figure 12). This general cooling occurs in spite of a coincident rise in solar irradiance forcing following the Maunder Minimum (circa 1645–1715) (Figure 12). Although only resolved by a few coral records with skill in this interval, the

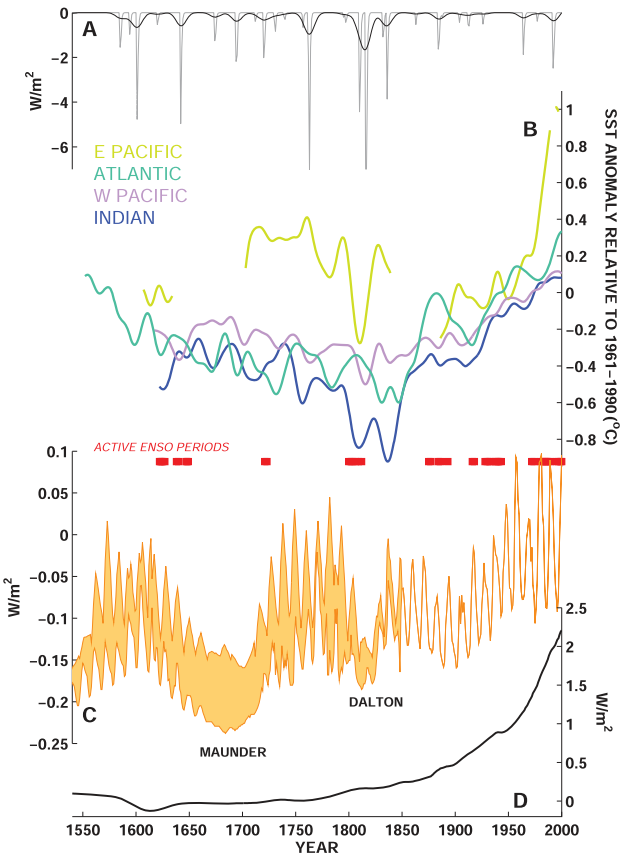

Figure 12. A comparison between the Ocean2K regional SST reconstructions and climate forcings of the last 400 years. (a) Volcanic forcing [*Gao et al.*, 2008]; annual time series in gray and a 20 year Gaussian smoothed time series in black; (b) the 20 year Gaussian smoothed best reconstructions from each basin; (c) solar forcing, with the thickness of the line representing the range of possible values, excluding the much larger range proposed by *Shapiro et al.* [2011]; (d) well-mixed greenhouse gases. Active ENSO periods, defined as where the amplitude of the 3–7 year band-pass filtered western Pacific reconstruction (c.f. Figure 8) exceeds 1.5 standard deviations, are marked in red. All radiative forcing data are derived from [*Schmidt et al.*, 2012]. The portions of the reconstructions that have an RE value equal to or below zero are not plotted.

Maunder Minimum does not seem to coincide with cooling in our reconstructions, suggesting that solar forcing played a minor role in forcing tropical SSTs. The cooling trend may instead be attributable to an increasing frequency of volcanic eruptions, which culminates in a pair of strong volcanic eruptions during the early 1800s, including the unknown eruption of 1809 and the Tambora eruption of 1815 [*Hansen et al.*, 2007; *Schmidt et al.*, 2012]. SSTs in the Indo-Pacific and the Atlantic reach their minimum observed values during the early 1800s, coincident with these eruptions as well as the Dalton solar minimum (Figure 12).

Warming in the Atlantic, western Pacific, and Indian Oceans begins near 1840, coincident with a recovery from volcanic forcing, an increase in total solar irradiance, and the initial rise in well-mixed greenhouse gases (Figure 12). These basins have warmed by about 0.6°C since 1850, in overall agreement with the instrumental record. The relatively early timing for the onset of warming likely reflects the recovery of ocean temperatures from (possibly volcanically induced) cooling in the early 1800s, rather than a direct response to early changes in greenhouse gas concentrations. However, rising greenhouse gases influenced tropical temperatures during the twentieth century [*Meehl et al.*, 2003; *Knutson et al.*, 2006; *Santer et al.*, 2006; *Knutson et al.*, 2013]. Indeed, for all basins, reconstructed temperatures for the most recent 50 years are higher than any other previous 50 year period (rank-sum test, $p < 0.01$ in all cases). As noted previously (section 4.3), however, the eastern Pacific reconstruction has a recent and apparently spurious warming trend, likely due to regional changes in surface water $\delta^{18}O$ and the subsequent effect on the $\delta^{18}O$ in the coral archives.

There have been extensive paleoclimate and model simulation-based investigations of the influence of both natural and anthropogenic forcings on ENSO mean state and variance [e.g., *Clement et al.*, 1999; *Cobb et al.*, 2003; *Mann et al.*, 2005; *Collins et al.*, 2010; *Cobb et al.*, 2013; *McGregor et al.*, 2013]. In particular, there are suggestions that ENSO may respond to external forcing from volcanic eruptions or solar variability, with volcanic eruptions enhancing ENSO variability [*Adams et al.*, 2003; *Mann et al.*, 2005] and increased solar forcing reducing it [*Emile-Geay et al.*, 2013b] consistent with the "ocean dynamical thermostat" hypothesis [*Clement et al.*, 1996]. Given the lack of long, continuous coral records from the eastern Pacific, our best assessment of how ENSO has changed in the past vis a vis climate forcings herein comes from the western Pacific region (Figure 8), in which SSTs vary with ENSO activity. Our western Pacific reconstruction suggests no consistent association between periods of high ENSO band variance and global-scale climatic forcings, natural or anthropogenic (Figure 12). A high-amplitude interval occurs near 1800—a globally cool

period—but high-amplitude variability also occurs during warm intervals, including during the late 1800s and 1900s. In addition, the early 1800s modulation begins well before the known volcanic eruptions at 1809 and 1815 (Figure 12), making it further unlikely that this period of enhanced ENSO activity was a direct result of volcanic forcing. This suggests that internal variability in the ENSO system is larger than the forced component over the last several centuries.

5. Conclusions

The regional, coral-based reconstructions of SST presented here expand our understanding of climate changes in the tropical surface ocean during the last four centuries. Interannual variance associated with ENSO activity has fluctuated substantially over the reconstruction intervals, but there is no clear evidence that solar, volcanic, or anthropogenic forcing caused these changes. Although decadal to multidecadal variability is a consistent feature of the western Atlantic record, variance in the ~70 year band associated with the AMO was apparently smaller prior to the nineteenth century; however, the limited validation skill in this basin prevents us from interpreting whether this result is robust.

Overall, we find that tropical ocean temperatures were cooling prior to the mid-1800s. The first few decades of the 1800s (1800–1820) were particularly cold periods in the Indian and western Pacific Ocean basins, coinciding with the large volcanic eruptions of 1809 and 1815 as well as the Dalton solar minimum. Around 1830–1840, significant warming began in the western Pacific, Indian Ocean, and western Atlantic. In the eastern tropical Pacific, multivariate, frequency-dependent, and possibly nonlinear influences on coral $\delta^{18}O$ observations suggest that trends in SST reconstructions from the region must be evaluated and interpreted with care. The other regions encompassed by our Indian, western Pacific, and western Atlantic targets have been warming since 1850 at an average rate of 0.04°C, 0.03°C, and 0.04°C per decade, respectively.

Additional annually resolved marine data that provide independent estimates of SST and seawater $\delta^{18}O$ or salinity variations, especially from the eastern tropical Pacific, will help to further assess recent thermal and hydrological changes in the tropical oceans. Future work to identify the mechanisms underlying reconstructed SST variations will rely on comparisons with the most recent Paleoclimate Modelling Intercomparison Project Phase 3 and Coupled Model Intercomparison Projects Phase 5, which include realistically forced simulations of both the last millennium (850–1850) and historical (1850 to present) climate, as well as comparisons with terrestrially based temperature reconstructions.

Acknowledgments

We are grateful to the many scientists who made their data sets publicly available via the PANGAEA and the World Data Center for Paleoclimatology electronic archives (pangaea.de,ncdc.noaa.gov/paleo). In 2012–2013, over 75 Ocean2k volunteers constructed the paleoclimate data metadatabase from which the data set studied here was developed (http://pages-igbp.org/workinggroups/ocean2k/data). Organizational and logistical support was provided by Thorsten Kiefer, Lucien von Gunten, and Christian Telepski (PAGES-IPO), via support from the U.S. NSF, NOAA, and the Swiss National Research Foundation. J.E.T. and K.J.A. acknowledge Woods Hole Oceanographic Institution for internal support. K.J.A. acknowledges the Frank and Lisina Hoch Endowed Fund at the Woods Hole Oceanographic Institution for support. N.J.A. is supported by an Australian Research Council QEII fellowship (DP110101161), and this research contributes to ARC Discovery Grant DP140102059. M.N.E. is supported by NSF/ATM0902794 and NSF/ATM0902715. J.Z. was supported by an Indian Ocean Marine Research Centre fellowship and an Honorary Research Fellowship by the University of the Witwatersrand. H.C.W. is supported by the Deutsche Forschungsgemeinschaft through DFG-Research Center/Cluster of Excellence "The Ocean in the Earth System" at the University of Bremen (MARUM Fellowship). C.G. acknowledges MARUM–Center for Marine Environmental Sciences for internal support. K.H.K. is supported by NOAA grant NA11OAR4310171. This is University of Maryland Center for Environmental Science contribution 4984. The paleoclimate data and reconstructions associated with this manuscript are available for download at the NOAA National Climatic Data Center Paleoclimatology website: http://www.ncdc.noaa.gov/paleo/study/17955.

References

Abram, N. J., M. K. Gagan, J. E. Cole, W. S. Hantoro, and M. Mudelsee (2008), Recent intensification of tropical climate variability in the Indian Ocean, *Nat. Geosci.*, *1*(12), 849–853.

Abram, N. J., H. V. McGregor, M. K. Gagan, W. S. Hantoro, and B. W. Suwargadi (2009), Oscillations in the southern extent of the Indo-Pacific Warm Pool during the mid-Holocene, *Quat. Sci. Rev.*, *28*(25), 2794–2803.

Adams, J. B., M. E. Mann, and C. M. Ammann (2003), Proxy evidence for an El Niño-like response to volcanic forcing, *Nature*, *426*(6964), 274–278.

Alibert, C., and L. Kinsley (2008), A 170-year Sr/Ca and Ba/Ca coral record from the western Pacific warm pool: 1. What can we learn from an unusual coral record?, *J. Geophys. Res.*, *113*, C04008, doi:10.1029/2006JC003979.

An, S.-I., J.-W. Kim, S.-H. Im, B.-M. Kim, and J.-H. Park (2012), Recent and future sea surface temperature trends in tropical Pacific warm pool and cold tongue regions, *Clim. Dyn.*, *39*(6), 1373–1383.

Anand, P., H. Elderfield, and M. H. Conte (2003), Calibration of Mg/Ca thermometry in planktonic foraminifera from a sediment trap time series, *Paleoceanography*, *18*(2), 1050, doi:10.1029/2002PA000846.

Anchukaitis, K. J., R. D. D'Arrigo, L. Andreu-Hayles, D. Frank, A. Verstege, A. Curtis, B. M. Buckley, G. C. Jacoby, and E. R. Cook (2013), Tree-ring-reconstructed summer temperatures from Northwestern North America during the last nine centuries, *J. Clim.*, *26*(10), 3001–3012, doi:10.1175/JCLI-D-11-00139.1.

Asami, R., T. Yamada, Y. Iryu, T. M. Quinn, C. P. Meyer, and G. Paulay (2005), Interannual and decadal variability of the western Pacific sea surface condition for the years 1787–2000: Reconstruction based on stable isotope record from a Guam coral, *J. Geophys. Res.*, *110*, C05018, doi:10.1029/2004JC002555.

Ault, T. R., J. E. Cole, M. N. Evans, H. Barnett, N. J. Abram, A. W. Tudhope, and B. K. Linsley (2009), Intensified decadal variability in tropical climate during the late 19th century, *Geophys. Res. Lett.*, *36*, L08602, doi:10.1029/2008GL036924.

Bagnato, S., B. K. Linsley, S. S. Howe, G. M. Wellington, and J. Salinger (2005), Coral oxygen isotope records of interdecadal climate variations in the South Pacific Convergence Zone region, *Geochem. Geophys. Geosyst.*, *6*, Q06001, doi:10.1029/2004GC000879.

Black, D. E., M. A. Abahazi, R. C. Thunell, A. Kaplan, E. J. Tappa, and L. C. Peterson (2007), An 8-century tropical Atlantic SST record from the Cariaco Basin: Baseline variability, twentieth-century warming, and Atlantic hurricane frequency, *Paleoceanography*, *22*, PA4204, doi:10.1029/2007PA001427.

Boiseau, M., A. Juillet-Leclerc, P. Yiou, B. Salvat, P. Isdale, and M. Guillaume (1998), Atmospheric and oceanic evidences of El Niño-Southern Oscillation events in the south central Pacific Ocean from coral stable isotopic records over the last 137 years, *Paleoceanography*, *13*(6), 671–685.

Boiseau, M., M. Ghil, and A. Juillet-Leclerc (1999), Climatic trends and interdecadal variability from south-central Pacific coral records, *Geophys. Res. Lett.*, *26*(18), 2881–2884.

Bottomley, M., C. K. Folland, J. Hsiung, R. E. Newell, and D. E. Parker (1990), *Global Ocean Surface Temperature Atlas*, Her Majesty's Str. Off., Norwich, England, U. K.
Cane, M. A., A. C. Clement, A. Kaplan, Y. Kushnir, R. Murtugudde, D. Pozdnyakov, R. Seager, and S. E. Zebiak (1997), 20th century sea surface temperature trends, *Science*, *275*, 957–960.
Charles, C., D. Hunter, and R. G. Fairbanks (1997), Interaction between the ENSO and the Asian monsoon in a coral record of tropical climate, *Science*, *277*(5328), 925–928.
Charles, C. D., K. Cobb, M. D. Moore, and R. G. Fairbanks (2003), Monsoon–tropical ocean interaction in a network of coral records spanning the 20th century, *Mar. Geol.*, *201*(1), 207–222.
Chaudhuri, P., and J. S. Marron (1999), SiZer for exploration of structures in curves, *J. Am. Stat. Assoc.*, *94*(447), 807–823.
Clement, A., R. Seager, and M. Cane (1999), Orbital controls on the El Niño/Southern Oscillation and the tropical climate, *Paleoceanography*, *14*(4), 441–456.
Clement, A. C., R. Seager, M. A. Cane, and S. E. Zebiak (1996), An ocean dynamical thermostat, *J. Clim.*, *9*(9), 2190–2196.
Cobb, K. M., C. D. Charles, and D. E. Hunter (2001), A central tropical Pacific coral demonstrates Pacific, Indian, and Atlantic decadal climate connections, *Geophys. Res. Lett.*, *28*(11), 2209–2212.
Cobb, K. M., C. D. Charles, H. Cheng, and R. L. Edwards (2003), El Niño/Southern Oscillation and tropical Pacific climate during the last millennium, *Nature*, *424*(6946), 271–276.
Cobb, K. M., N. Westphal, H. R. Sayani, J. T. Watson, E. Di Lorenzo, H. Cheng, R. Edwards, and C. D. Charles (2013), Highly variable El Niño–Southern Oscillation throughout the Holocene, *Science*, *339*(6115), 67–70.
Cohen, A. L., G. D. Layne, S. R. Hart, and P. S. Lobel (2001), Kinetic control of skeletal Sr/Ca in a symbiotic coral: Implications for the paleotemperature proxy, *Paleoceanography*, *16*(1), 20–26.
Cole, J. E., and E. R. Cook (1998), The changing relationship between ENSO variability and moisture balance in the continental United States, *Geophys. Res. Lett.*, *25*, 4529–4532.
Cole, J. E., and R. G. Fairbanks (1990), The Southern Oscillation recorded in the δ^{18}O of corals from Tarawa Atoll, *Paleoceanography*, *5*(5), 669–683.
Cole, J. E., R. G. Fairbanks, and G. T. Shen (1993), Recent variability in the Southern Oscillation: Isotopic results from a Tarawa Atoll coral, *Science*, *260*(5115), 1790–1793.
Cole, J. E., R. B. Dunbar, T. R. McClanahan, and N. A. Muthiga (2000), Tropical Pacific forcing of decadal SST variability in the western Indian Ocean over the past two centuries, *Science*, *287*(5453), 617–619.
Collins, M., et al. (2010), The impact of global warming on the tropical Pacific Ocean and El Niño, *Nat. Geosci.*, *3*(6), 391–397.
Comboul, M., J. Emile-Geay, M. Evans, N. Mirnateghi, K. M. Cobb, and D. M. Thompson (2014), A probabilistic model of chronological errors in layer-counted climate proxies: Applications to annually banded coral archives, *Clim. Past*, *10*(2), 825–841.
Cook, E. R., D. M. Meko, D. W. Stahle, and M. K. Cleaveland (1999), Drought reconstructions for the continental United States, *J. Clim.*, *12*, 1145–1162.
Cook, E. R., R. D. D'Arrigo, and M. E. Mann (2002), A well-verified, multiproxy reconstruction of the winter North Atlantic Oscillation Index since AD 1400, *J. Clim.*, *15*(13), 1754–1764.
Cook, E. R., K. J. Anchukaitis, B. M. Buckley, R. D. D'Arrigo, G. C. Jacoby, and W. E. Wright (2010), Asian monsoon failure and megadrought during the last millennium, *Science*, *328*(5977), 486–489, doi:10.1126/science.1185188.
Cooper, T. F., R. A. O'Leary, and J. M. Lough (2012), Growth of Western Australian corals in the Anthropocene, *Science*, *335*(6068), 593–596, doi:10.1126/science.1214570.
Damassa, T. D., J. E. Cole, H. R. Barnett, T. R. Ault, and T. R. McClanahan (2006), Enhanced multidecadal climate variability in the seventeenth century from coral isotope records in the western Indian Ocean, *Paleoceanography*, *21*, PA2016, doi:10.1029/2005PA001217.
D'Arrigo, R., R. Wilson, J. Palmer, P. Krusic, A. Curtis, J. Sakulich, S. Bijaksana, S. Zulaikah, L. O. Ngkoimani, and A. Tudhope (2006), The reconstructed Indonesian warm pool sea surface temperatures from tree rings and corals: Linkages to Asian monsoon drought and El Niño–Southern Oscillation, *Paleoceanography*, *21*, PA3005, doi:10.1029/2005PA001256.
de Villiers, S., G. T. Shen, and B. K. Nelson (1994), The Sr/Ca-temperature relationship in coralline aragonite—Influence of variability in $Sr/Ca_{seawater}$ and skeletal growth parameters, *Geochim. Cosmochim. Acta*, *58*, 197–208, doi:10.1016/0016-7037(94)90457-X.
De'ath, G., J. M. Lough, and K. E. Fabricius (2009), Declining coral calcification on the Great Barrier Reef, *Science*, *323*(5910), 116–119.
Delcroix, T., S. Cravatte, and M. J. McPhaden (2007), Decadal variations and trends in tropical Pacific sea surface salinity since 1970, *J. Geophys. Res.*, *112*, C03012, doi:10.1029/2006JC003801.
DeLong, K. L., T. M. Quinn, F. W. Taylor, K. Lin, and C.-C. Shen (2012), Sea surface temperature variability in the southwest tropical Pacific since AD 1649, *Nat. Clim. Change*, *2*, 799–804.
DeLong, K. L., T. M. Quinn, F. W. Taylor, C.-C. Shen, and K. Lin (2013), Improving coral-base paleoclimate reconstructions by replicating 350 years of coral Sr/Ca variations, *Palaeogeogr. Palaeoclimatol. Palaeoecol.*, *373*, 6–24.
DeLong, K. L., J. A. Flannery, R. Z. Poore, T. M. Quinn, C. R. Maupin, K. Lin, and C.-C. Shen (2014), A reconstruction of sea surface temperature variability in the southeastern Gulf of Mexico from 1734 to 2008 C.E. using cross-dated Sr/Ca records from the coral Siderastrea siderea, *Paleoceanography*, *29*, 403–422, doi:10.1002/2013PA002524.
Diaz, H. F., M. P. Hoerling, and J. K. Eischeid (2001), ENSO variability, teleconnections and climate change, *Int. J. Climatol.*, *21*(15), 1845–1862.
Dommenget, D., T. Bayr, and C. Frauen (2012), Analysis of the non-linearity in the pattern and time evolution of El Niño Southern Oscillation, *Clim. Dyn.*, *40*(11–12), 2825–2847, doi:10.1007/s00382-012-1475-0.
Druffel, E. R., and S. Griffin (1999), Variability of surface ocean radiocarbon and stable isotopes in the southwestern Pacific, *J. Geophys. Res.*, *104*(C10), 23,607–23,613.
Dunbar, R. B., and J. E. Cole (Eds.) (1999), *Annual Records of Tropical Systems: Recommendations for Research*. 99-1, PAGES/CLIVAR PAGES, Past Global Changes.
Dunbar, R. B., G. M. Wellington, M. W. Colgan, and P. W. Glynn (1994), Eastern Pacific sea surface temperature since 1600 AD: The δ^{18}O record of climate variability in Galapagos corals, *Paleoceanography*, *9*(2), 291–315.
Durack, P. J., and S. E. Wijffels (2010), Fifty-year trends in global ocean salinities and their relationship to broad-scale warming, *J. Clim.*, *23*(16), 4342–4362.
Ebisuzaki, W. (1997), A method to estimate the statistical significance of a correlation when the data are serially correlated, *J. Clim.*, *10*(9), 2147–2153.
Emile-Geay, J., K. M. Cobb, M. E. Mann, and A. T. Wittenberg (2013a), Estimating central equatorial Pacific SST variability over the past millennium: Part I. Methodology and validation, *J. Clim.*, *26*(7), 2302–2328.

Emile-Geay, J., K. M. Cobb, M. E. Mann, and A. T. Wittenberg (2013b), Estimating central equatorial Pacific SST variability over the past millennium: Part II. Reconstructions and implications, *J. Clim.*, *26*(7), 2329–2352.
Enfield, D. B., and D. A. Mayer (1997), Tropical Atlantic sea surface temperature variability and its relation to El Niño-Southern Oscillation, *J. Geophys. Res.*, *102*(C1), 929–945.
Esper, J., E. R. Cook, and F. H. Schweingruber (2002), Low-frequency signals in long tree-ring chronologies for reconstructing past temperature variability, *Science*, *295*, 2250–2253.
Esper, J., D. C. Frank, R. J. S. Wilson, and K. R. Briffa (2005), Effect of scaling and regression on reconstructed temperature amplitude for the past millennium, *Geophys. Res. Lett.*, *32*, L07711, doi:10.1029/2004GL021236.
Evans, M. N., R. G. Fairbanks, and J. L. Rubenstone (1999), The thermal oceanographic signal of El Niño reconstructed from a Kiritimati Island coral, *J. Geophys. Res.*, *104*, 13,409–13,421.
Evans, M. N., A. Kaplan, and M. A. Cane (2000), Intercomparison of coral oxygen isotope data and historical Sea Surface Temperature (SST): Potential for coral-based SST field reconstructions, *Paleoceanography*, *15*(5), 551–563.
Evans, M. N., A. Kaplan, and M. A. Cane (2002), Pacific sea surface temperature field reconstruction from coral δ^{18}O data using reduced space objective analysis, *Paleoceanography*, *17*(1), 7-1–7-13, doi:10.1029/2000PA000590.
Fairbanks, R. G., M. N. Evans, J. L. Rubenstone, R. A. Mortlock, K. Broad, M. D. Moore, and C. D. Charles (1997), Evaluating climate indices and their geochemical proxies measured in corals, *Coral Reefs*, *16*, S93–S100.
Fedorov, A. V., and S. G. Philander (2000), Is El Niño changing?, *Science*, *288*(5473), 1997–2002.
Felis, T., J. Pätzold, Y. Loya, M. Fine, A. H. Nawar, and G. Wefer (2000), A coral oxygen isotope record from the northern Red Sea documenting NAO, ENSO, and North Pacific teleconnections on Middle East climate variability since the year 1750, *Paleoceanography*, *15*(6), 679–694.
Felis, T., G. Lohmann, H. Kuhnert, S. J. Lorenz, D. Scholz, J. Pätzold, S. A. Al-Rousan, and S. M. Al-Moghrabi (2004), Increased seasonality in Middle East temperatures during the last interglacial period, *Nature*, *429*(6988), 164–168.
Felis, T., A. Suzuki, H. Kuhnert, M. Dima, G. Lohmann, and H. Kawahata (2009), Subtropical coral reveals abrupt early-twentieth-century freshening in the western North Pacific Ocean, *Geology*, *37*(6), 527–530.
Frank, D. C., J. Esper, C. C. Raible, U. Büntgen, V. Trouet, B. Stocker, and F. Joos (2010), Ensemble reconstruction constraints on the global carbon cycle sensitivity to climate, *Nature*, *463*(7280), 527–530, doi:10.1038/nature08769.
Gagan, M. K., L. K. Ayliffe, D. Hopley, J. A. Cali, G. E. Mortimer, J. Chappell, M. T. McCulloch, and M. J. Head (1998), Temperature and surface-ocean water balance of the mid-Holocene tropical western Pacific, *Science*, *279*(5353), 1014–1018.
Gagan, M. K., L. K. Ayliffe, J. W. Beck, J. E. Cole, E. R. M. Druffel, R. B. Dunbar, and D. P. Schrag (2000), New views of tropical paleoclimates from corals, *Quat. Sci. Rev.*, *19*, 45–64.
Gagan, M. K., G. B. Dunbar, and A. Suzuki (2012), The effect of skeletal mass accumulation in Porites on coral Sr/Ca and δ^{18}O paleothermometry, *Paleoceanography*, *27*, PA1203, doi:10.1029/2011PA002215.
Gallant, A. J. E., S. J. Phipps, D. J. Karoly, A. B. Mullan, and A. M. Lorrey (2013), Nonstationary Australasian teleconnections and implications for paleoclimate reconstructions, *J. Clim.*, *26*(22), 8827–8849, doi:10.1175/jcli-d-12-00338.1.
Gao, C., A. Robock, and C. Ammann (2008), Volcanic forcing of climate over the past 1500 years: An improved ice core-based index for climate models, *J. Geophys. Res.*, *113*, D23111, doi:10.1029/2008JD010239.
Gershunov, A., and T. P. Barnett (1998), Interdecadal modulation of ENSO teleconnections, *Bull. Am. Meteorol. Soc.*, *79*(12), 2715–2725.
Gill, A. E. (1982), *Atmosphere–Ocean Dynamics, International Geophysics*, 662 pp., Academic, New York.
Gill, A. E., and E. Rasmusson (1983), The 1982–83 climate anomaly in the equatorial Pacific, *Nature*, *306*(5940), 229–234.
Giry, C., T. Felis, M. Kölling, D. Scholz, W. Wei, G. Lohmann, and S. Scheffers (2012), Mid-to late Holocene changes in tropical Atlantic temperature seasonality and interannual to multidecadal variability documented in southern Caribbean corals, *Earth Planet. Sci. Lett.*, *331*, 187–200.
Goodkin, N. F., K. A. Hughen, W. B. Curry, S. C. Doney, and D. R. Ostermann (2008), Sea surface temperature and salinity variability at Bermuda during the end of the Little Ice Age, *Paleoceanography*, *23*, PA3203, doi:10.1029/2007PA001532.
Gorman, M. K., T. M. Quinn, F. W. Taylor, J. W. Partin, G. Cabioch, J. A. Austin, B. Pelletier, V. Ballu, C. Maes, and S. Saustrup (2012), A coral-based reconstruction of sea surface salinity at Sabine Bank, Vanuatu from 1842 to 2007 CE, *Paleoceanography*, *27*, PA3226, doi:10.1029/2012PA002302.
Gray, S. T., L. J. Graumlich, J. L. Betancourt, and G. T. Pederson (2004), A tree-ring based reconstruction of the Atlantic Multidecadal Oscillation since 1567 AD, *Geophys. Res. Lett.*, *31*, L12205, doi:10.1029/2004GL019932.
Grossman, E. L., and T.-L. Ku (1986), Oxygen and carbon isotopic fractionation in biogenic aragonite: Temperature effects, *Chem. Geol.*, *59*, 59–74.
Guilderson, T. P., and D. P. Schrag (1999), Reliability of coral isotope records from the Western Pacific Warm Pool: A comparison using age-optimized records, *Paleoceanography*, *14*(4), 457–464.
Hansen, J., et al. (2007), Climate simulations for 1880–2003 with GISS modelE, *Clim. Dyn.*, *29*, 661–696, doi:10.1007/s00382-007-0255-8.
Hegerl, G. C., T. J. Crowley, M. Allen, W. T. Hyde, H. N. Pollack, J. Smerdon, and E. Zorita (2007), Detection of human influence on a new, validated 1500-year temperature reconstruction, *J. Clim.*, *20*(4), 650–666.
Heiss, G. A. (1994), Coral reefs in the Red Sea: Growth, production, and stable isotopes, *Tech. Rep. 32*, GEOMAR, Research Center for Marine Geosciences Christian Albrechts University.
Held, I. M., and B. J. Soden (2006), Robust responses of the hydrological cycle to global warming, *J. Clim.*, *19*(21), 5686–5699.
Hendy, E., M. Gagan, J. Lough, M. McCulloch, and P. deMenocal (2007), Impact of skeletal dissolution and secondary aragonite on trace element and isotopic climate proxies in Porites corals, *Paleoceanography*, *22*, PA4101, doi:10.1029/2007PA001462.
Hetzinger, S., M. Pfeiffer, W.-C. Dullo, D. Garbe-Schönberg, and J. Halfar (2010), Rapid 20th century warming in the Caribbean and impact of remote forcing on climate in the northern tropical Atlantic as recorded in a Guadeloupe coral, *Palaeogeogr. Palaeoclimatol. Palaeoecol.*, *296*(1), 111–124.
Ingleby, B., and M. Huddleston (2007), Quality control of ocean temperature and salinity profiles–Historical and real-time data, *J. Mar. Syst.*, *65*(1), 158–175.
Isdale, P., B. Stewart, K. Tickle, and J. Lough (1998), Palaeohydrological variation in a tropical river catchment: A reconstruction using fluorescent bands in corals of the Great Barrier Reef, Australia, *Holocene*, *8*(1), 1–8.
Juillet-Leclerc, A., S. Reynaud, D. Dissard, G. Tisserand, and C. Ferrier-Pagès (2014), Light is an active contributor to the vital effects of coral skeleton proxies, *Geochim. Cosmochim. Acta*, *140*, 671–690, doi:10.1016/j.gca.2014.05.042.
Kaplan, A., M. A. Cane, Y. Kushnir, A. C. Clement, M. B. Blumenthal, and B. Rajagopalan (1998), Analyses of global sea surface temperature 1856–1991, *J. Geophys. Res.*, *103*(C9), 18,567–18,589.

Kilbourne, K. H., T. M. Quinn, F. W. Taylor, T. Delcroix, and Y. Gouriou (2004), El Niño-Southern Oscillation-related salinity variations recorded in the skeletal geochemistry of a Porites coral from Espiritu Santo, Vanuatu, *Paleoceanography*, *19*, PA4002, doi:10.1029/2004PA001033.

Kilbourne, K. H., T. Quinn, R. Webb, T. Guilderson, J. Nyberg, and A. Winter (2008), Paleoclimate proxy perspective on Caribbean climate since the year 1751: Evidence of cooler temperatures and multidecadal variability, *Paleoceanography*, *23*, PA3220, doi:10.1029/2008PA001598.

Kilbourne, K. H., M. A. Alexander, and J. A. Nye (2014), A low latitude paleoclimate perspective on Atlantic multidecadal variability, *J. Mar. Syst.*, *133*, 4–13, doi:10.1016/j.jmarsys.2013.09.004.

Kinsman, D. J. J., and H. D. Holland (1969), The co-precipitation of cations with $CaCO_3$—IV. The co-precipitation of Sr^{2+} with aragonite between 16° and 96°C, *Geochim. Cosmochim. Acta*, *33*, 1–17.

Knight, J. R., R. J. Allan, C. K. Folland, M. Vellinga, and M. E. Mann (2005), A signature of persistent natural thermohaline circulation cycles in observed climate, *Geophys. Res. Lett.*, *32*, L20708, doi:10.1029/2005GL024233.

Knippertz, P., U. Ulbrich, F. Marques, and J. Corte-Real (2003), Decadal changes in the link between El Niño and springtime North Atlantic Oscillation and European-North African rainfall, *Int. J. Climatol.*, *23*(11), 1293–1311, doi:10.1002/joc.944.

Knutson, T. R., T. L. Delworth, K. W. Dixon, I. M. Held, J. Lu, V. Ramaswamy, M. D. Schwarzkopf, G. Stenchikov, and R. J. Stouffer (2006), Assessment of twentieth-century regional surface temperature trends using the GFDL CM2 coupled models, *J. Clim.*, *19*(9), 1624–1651, doi:10.1175/jcli3709.1.

Knutson, T. R., F. Zeng, and A. T. Wittenberg (2013), Multimodel assessment of regional surface temperature trends: CMIP3 and CMIP5 twentieth-century simulations, *J. Clim.*, *26*(22), 8709–8743.

Kuhnert, H., J. Pätzold, B. Hatcher, K.-H. Wyrwoll, A. Eisenhauer, L. Collins, Z. Zhu, and G. Wefer (1999), A 200-year coral stable oxygen isotope record from a high-latitude reef off Western Australia, *Coral Reefs*, *18*(1), 1–12.

Kuhnert, H., J. Pätzold, K.-H. Wyrwoll, and G. Wefer (2000), Monitoring climate variability over the past 116 years in coral oxygen isotopes from Ningaloo Reef, Western Australia, *Int. J. Earth Sci.*, *88*(4), 725–732.

Kuhnert, H., T. Crüger, and J. Pätzold (2005), NAO signature in a Bermuda coral Sr/Ca record, *Geochem. Geophys. Geosyst.*, *6*, Q04004, doi:10.1029/2004GC000786.

Kumar, A., and M. P. Hoerling (1998), Annual cycle of Pacific-North American seasonal predictability associated with different phases of ENSO, *J. Clim.*, *11*(12), 3295–3308.

Landrum, L., B. L. Otto-Bliesner, E. R. Wahl, A. Conley, P. J. Lawrence, N. Rosenbloom, and H. Teng (2013), Last millennium climate and its variability in CCSM4, *J. Clim.*, *26*(4), 1085–1111, doi:10.1175/jcli-d-11-00326.1.

Lea, D. W., T. A. Mashiotta, and H. J. Spero (1999), Controls on magnesium and strontium uptake in planktonic foraminifera determined by live culturing, *Geochim. Cosmochim. Acta*, *63*(16), 2369–2379.

Leder, J., P. K. Swart, A. Szmant, and R. Dodge (1996), The origin of variations in the isotopic record of scleractinian corals: I. Oxygen, *Geochim. Cosmochim. Acta*, *60*(15), 2857–2870.

LeGrande, A. N., and G. A. Schmidt (2006), Global gridded data set of the oxygen isotopic composition in seawater, *Geophys. Res. Lett.*, *33*, L12604, doi:10.1029/2006GL026011.

Linsley, B. K., R. B. Dunbar, G. M. Wellington, and D. A. Mucciarone (1994), A coral-based reconstruction of Intertropical Convergence Zone variability over Central America since 1707, *J. Geophys. Res.*, *99*(C5), 9977–9994.

Linsley, B. K., L. Ren, R. B. Dunbar, and S. S. Howe (2000), El Niño Southern Oscillation (ENSO) and decadal-scale climate variability at 10°N in the eastern Pacific from 1893 to 1994: A coral-based reconstruction from Clipperton Atoll, *Paleoceanography*, *15*(3), 322–335.

Linsley, B. K., A. Kaplan, Y. Gouriou, J. Salinger, P. B. Demenocal, G. M. Wellington, and S. S. Howe (2006), Tracking the extent of the South Pacific Convergence Zone since the early 1600s, *Geochem. Geophys. Geosyst.*, *7*, Q05003, doi:10.1029/2005GC001115.

Locarnini, R. A., A. V. Mishonov, J. I. Antonov, T. P. Boyer, H. E. Garcia, O. K. Baranova, M. M. Zweng, and D. R. Johnson (2010), World Ocean Atlas 2009: Volume 1. Temperature, in *NOAA Atlas NESDIS*, vol. 68, edited by S. Levitus, pp. 1–184, U.S. Gov. Print. Off., Washington, D. C.

López-Parages, J., and B. Rodríguez-Fonseca (2012), Multidecadal modulation of El Niño influence on the Euro-Mediterranean rainfall, *Geophys. Res. Lett.*, *39*, L02704, doi:10.1029/2011GL050049.

Lough, J. M. (2004), A strategy to improve the contribution of coral data to high-resolution paleoclimatology, *Palaeogeogr. Palaeoclimatol. Palaeoecol.*, *204*(1-2), 115–143.

Lough, J. M. (2010), Climate records from corals, *WIREs Clim. Change*, *1*(3), 318–331, doi:10.1002/wcc.39.

Lough, J. M., and D. J. Barnes (1997), Several centuries of variation in skeletal extension, density, and calcification in massive Porites colonies from the Great Barrier Reef: A proxy for seawater temperature and a background of variability against which to identify unnatural change, *J. Exper. Mar. Biol. Ecol.*, *211*, 29–67.

Lough, J. M., and T. F. Cooper (2011), New insights from coral growth band studies in an era of rapid environmental change, *Earth Sci. Rev.*, *108*(3), 170–184.

Lough, J. M., D. Barnes, and F. McAllister (2002), Luminescent lines in corals from the Great Barrier Reef provide spatial and temporal records of reefs affected by land runoff, *Coral Reefs*, *21*(4), 333–343.

Mann, M. E., and K. A. Emanuel (2006), Atlantic hurricane trends linked to climate change, *Eos Trans. AGU*, *87*(24), 233–241, doi:10.1029/2006EO240001.

Mann, M. E., M. A. Cane, S. E. Zebiak, and A. Clement (2005), Volcanic and solar forcing of the tropical pacific over the past 1000 years, *J. Clim.*, *18*(3), 447–456.

Mann, M. E., Z. Zhang, S. Rutherford, R. S. Bradley, M. K. Hughes, D. Shindell, C. Ammann, G. Faluvegi, and F. Ni (2009), Global signatures and dynamical origins of the Little Ice Age and Medieval Climate Anomaly, *Science*, *326*(5957), 1256–1260.

Masson-Delmotte, V., et al. (2013), Information from paleoclimate archives, in *Climate Change 2013: The Physical Science Basis. Contribution of Working Group I to the Fifth Assessment Report of the Intergovernmental Panel on Climate Change*, edited by T. F. Stocker et al., pp. 383–464, Cambridge Univ. Press, Cambridge, U. K., and New York.

McCulloch, M., S. Fallon, T. Wyndham, E. Hendy, J. Lough, and D. Barnes (2003), Coral record of increased sediment flux to the inner Great Barrier Reef since European settlement, *Nature*, *421*(6924), 727–730.

McCulloch, M. T., M. K. Gagan, G. E. Mortimer, A. R. Chivas, and P. J. Isdale (1994), A high-resolution Sr/Ca and $\delta^{18}O$ coral record from the Great Barrier Reef, Australia, and the 1982–1983 El Niño, *Geochim. Cosmochim. Acta*, *58*(12), 2747–2754.

McGregor, H. V., and N. J. Abram (2008), Images of diagenetic textures in Porites corals from Papua New Guinea, *Geochem. Geophys. Geosyst.*, *9*, Q10013, doi:10.1029/2008GC002093.

McGregor, H. V., and M. K. Gagan (2003), Diagenesis and geochemistry of Porites corals from Papua New Guinea: Implications for paleoclimate reconstruction, *Geochem. Geophys. Geosyst.*, *67*(12), 2147–2156, doi:10.1016/S0016-7037(02)01050-5.

McGregor, H. V., M. Fischer, M. Gagan, D. Fink, S. Phipps, H. Wong, and C. Woodroffe (2013), A weak El Niño/Southern Oscillation with delayed seasonal growth around 4,300 years ago, *Nat. Geosci.*, *6*(11), 949–953.
Meehl, G. A., W. M. Washington, T. M. L. Wigley, J. M. Arblaster, and A. Dai (2003), Solar and greenhouse gas forcing and climate response in the twentieth century, *J. Clim.*, *16*(3), 426–444.
Meko, D. (1997), Dendroclimatic reconstruction with time varying predictor subsets of tree indices, *J. Clim.*, *10*(4), 687–696.
Morrissey, M. L., and N. E. Graham (1996), Recent trends in rain gauge precipitation measurements from the tropical Pacific: Evidence for an enhanced hydrologic cycle, *Bull. Am. Meteorol. Soc.*, *77*(6), 1207–1219.
Moustafa, Y. (2000), Paleoclimatic reconstructions of the northern Red Sea during the Holocene inferred from stable isotope records of modern and fossil corals and molluscs, PhD thesis, Berichte aus dem Fachbereich Geowissenschaften der Universität Bremen, Bremen, Germany.
Mullan, A. B. (1995), On the linearity and stability of Southern Oscillation-climate relationships for New Zealand, *Int. J. Climatol.*, *15*(12), 1365–1386, doi:10.1002/joc.3370151205.
Nakamura, N., H. Kayanne, H. Iijima, T. R. McClanahan, S. K. Behera, and T. Yamagata (2009), Mode shift in the Indian Ocean climate under global warming stress, *Geophys. Res. Lett.*, *36*, L23708, doi:10.1029/2009GL040590.
Newman, M., G. P. Compo, and M. A. Alexander (2003), ENSO-forced variability of the Pacific decadal oscillation, *J. Clim.*, *16*(23), 3853–3857.
Nurhati, I. S., K. M. Cobb, C. D. Charles, and R. B. Dunbar (2009), Late 20th century warming and freshening in the central tropical Pacific, *Geophys. Res. Lett.*, *36*, L21606, doi:10.1029/2009GL040270.
Nurhati, I. S., K. M. Cobb, and E. Di Lorenzo (2011), Decadal-scale SST and salinity variations in the central Tropical Pacific: Signatures of natural and anthropogenic climate change, *J. Clim.*, *24*(13), 3294–3308.
Oppo, D. W., Y. Rosenthal, and B. K. Linsley (2009), 2,000-year-long temperature and hydrology reconstructions from the Indo-Pacific warm pool, *Nature*, *460*(7259), 1113–1116.
Osborne, M. C., R. B. Dunbar, D. A. Mucciarone, E. Druffel, and J.-A. Sanchez-Cabeza (2014), A 215-yr coral $\delta^{18}O$ time series from Palau records dynamics of the West Pacific Warm Pool following the end of the Little Ice Age, *Coral Reefs*, *33*, 719–731, doi:10.1007/s00338-014-1146-1.
Past Global Changes 2k Consortium (2013), Continental-scale temperature variability during the past two millennia, *Nat. Geosci.*, *6*, 339–346.
Parker, D. E., P. D. Jones, C. K. Folland, and A. Bevan (1994), Interdecadal changes of surface temperature since the late nineteenth century, *J. Geophys. Res.*, *99*, 14,373–14,399.
Percival, D. B., and A. T. Walden (1993), *Spectral analysis for physical applications*, Cambridge Univ. Press, Cambridge, U. K., doi: 10.1017/cbo9780511622762.
Pfeiffer, M., O. Timm, W.-C. Dullo, and S. Podlech (2004), Oceanic forcing of interannual and multidecadal climate variability in the southwestern Indian Ocean: Evidence from a 160 year coral isotopic record (La Réunion, 55 E, 21 S), *Paleoceanography*, *19*, PA4006, doi:10.1029/2003PA000964.
Pfeiffer, M., W.-C. Dullo, J. Zinke, and D. Garbe-Schönberg (2009), Three monthly coral Sr/Ca records from the Chagos Archipelago covering the period of 1950–1995 AD: Reproducibility and implications for quantitative reconstructions of sea surface temperature variations, *Int. J. Earth Sci.*, *98*(1), 53–66.
Priestley, M. B. (1965), Evolutionary spectra and non-stationary processes, *J. R. Stat. Soc. B*, *27*, 204–237.
Quinn, T. M., T. J. Crowley, and F. W. Taylor (1996), New stable isotope results from a 173-year coral from Espiritu Santo, Vanuatu, *Geophys. Res. Lett.*, *23*(23), 3413–3416.
Quinn, T. M., T. J. Crowley, F. W. Taylor, C. Henin, P. Joannot, and Y. Join (1998), A multicentury stable isotope record from a New Caledonia coral: Interannual and decadal sea surface temperature variability in the southwest Pacific since 1657 AD, *Paleoceanography*, *13*(4), 412–426.
Quinn, T. M., F. W. Taylor, and T. J. Crowley (2006), Coral-based climate variability in the Western Pacific Warm Pool since 1867, *J. Geophys. Res.*, *111*, C11006, doi:10.1029/2005JC003243.
Rajagopalan, B., E. Cook, U. Lall, and B. K. Ray (2000), Spatiotemporal variability of ENSO and SST teleconnections to summer drought over the United States during the twentieth century, *J. Clim.*, *13*(24), 4244–4255.
Rayner, N. A., D. E. Parker, E. B. Horton, C. K. Folland, L. V. Alexander, D. Rowell, E. Kent, and A. Kaplan (2003), Globally complete analyses of sea surface temperature, sea ice and night marine air temperature, 1871–2000, *J. Geophys. Res.*, *108*(D14), 4407, doi:10.1029/2002JD002670.
Rayner, N. A., P. Brohan, D. E. Parker, C. K. Folland, J. J. Kennedy, M. Vanicek, T. J. Ansell, and S. F. B. Tett (2006), Improved analyses of changes and uncertainties in sea surface temperature measured in situ since the mid-nineteenth century: The HadSST2 dataset, *J. Clim.*, *19*(3), 446–469, doi:10.1175/jcli3637.1.
Reynolds, R. W., and T. M. Smith (1994), Improved global sea surface temperature analyses using optimum interpolation, *J. Clim.*, *7*(6), 929–948.
Richey, J. N., R. Z. Poore, B. P. Flower, and T. M. Quinn (2007), 1400 yr multiproxy record of climate variability from the northern Gulf of Mexico, *Geology*, *35*(5), 423–426.
Richey, J. N., R. Z. Poore, B. P. Flower, T. M. Quinn, and D. J. Hollander (2009), Regionally coherent Little Ice Age cooling in the Atlantic warm pool, *Geophys. Res. Lett.*, *36*, L21703, doi:10.1029/2009GL040445.
Ropelewski, C. F., and M. S. Halpert (1987), Global and regional scale precipitation patterns associated with the El Niño/Southern Oscillation, *Mon. Weather Rev.*, *114*, 2352–2362.
Saenger, C., A. L. Cohen, D. W. Oppo, R. B. Halley, and J. E. Carilli (2009), Surface-temperature trends and variability in the low-latitude North Atlantic since 1552, *Nat. Geosci.*, *2*(7), 492–495.
Santer, B. D., et al. (2006), Forced and unforced ocean temperature changes in Atlantic and Pacific tropical cyclogenesis regions, *Proc. Natl. Acad. Sci.*, *103*(38), 13,905–13,910, doi:10.1073/pnas.0602861103.
Schmidt, G. A., et al. (2012), Climate forcing reconstructions for use in PMIP simulations of the Last Millennium (v1.1), *Geosci. Model Dev.*, *5*(1), 185–191, doi:10.5194/gmd-5-185-2012.
Shanahan, T. M., J. T. Overpeck, K. J. Anchukaitis, J. W. Beck, J. E. Cole, D. L. Dettman, J. A. Peck, C. A. Scholz, and J. W. King (2009), Atlantic forcing of persistent drought in West Africa, *Science*, *324*(5925), 377–380.
Shapiro, A., W. Schmutz, E. Rozanov, M. Schoell, M. Haberreiter, A. Shapiro, and S. Nyeki (2011), A new approach to the long-term reconstruction of the solar irradiance leads to large historical solar forcing, *Astron. Astrophys.*, *529*, A67.
Shoemaker, L. H. (2003), Fixing the F test for equal variances, *Am. Stat.*, *57*(2), 105–114.

Smerdon, J. E., A. Kaplan, D. Chang, and M. N. Evans (2011), A pseudoproxy evaluation of the CCA and RegEM methods for reconstructing climate fields of the last millennium, *J. Clim.*, *24*(4), 1284–1309.
Smith, T. M., R. W. Reynolds, T. C. Peterson, and J. Lawrimore (2008), Improvements to NOAA's historical merged land-ocean surface temperature analysis (1880–2006), *J. Clim.*, *21*(10), 2283–2296.
Solomon, A., and M. Newman (2012), Reconciling disparate twentieth-century Indo-Pacific ocean temperature trends in the instrumental record, *Nat. Clim. Change*, *2*(9), 691–699.
Svendsen, L., S. Hetzinger, N. Keenlyside, and Y. Gao (2014), Marine-based multiproxy reconstruction of Atlantic multidecadal variability, *Geophys. Res. Lett.*, *41*(4), 1295–1300, doi:10.1002/2013GL059076.
Swart, P., H. Elderfield, and M. Greaves (2002), A high-resolution calibration of Sr/Ca thermometry using the Caribbean coral Montastraea annularis, *Geochem. Geophys. Geosyst.*, *3*(11), 8402, doi:10.1029/2002GC000306.
Swart, P. K., G. F. Healy, R. E. Dodge, P. Kramer, J. H. Hudson, R. B. Halley, and M. B. Robblee (1996a), The stable oxygen and carbon isotopic record from a coral growing in Florida Bay: A 160 year record of climatic and anthropogenic influence, *Palaeogeogr. Palaeoclimatol. Palaeoecol.*, *123*(1), 219–237.
Swart, P. K., R. E. Dodge, and H. J. Hudson (1996b), A 240-year stable oxygen and carbon isotopic record in a coral from South Florida: Implications for the prediction of precipitation in southern Florida, *Palaios*, *11*(4), 362–375.
Thompson, D. M., T. R. Ault, M. N. Evans, J. E. Cole, and J. Emile-Geay (2011), Comparison of observed and simulated tropical climate trends using a forward model of coral δ^{18}O, *Geophys. Res. Lett.*, *38*, L14706, doi:10.1029/2011GL048224.
Thomson, D. J. (1982), Spectrum estimation and harmonic analysis, *Proc. IEEE*, *70*, 1055–1096.
Trenberth, K. E., and J. W. Hurrell (1994), Decadal atmosphere-ocean variations in the Pacific, *Clim. Dyn.*, *9*(6), 303–319.
Tudhope, A. W., C. P. Chilcott, M. T. McCulloch, E. R. Cook, J. Chappell, R. M. Ellam, D. W. Lea, J. M. Lough, and G. B. Shimmield (2001), Variability in the El Niño-Southern Oscillation through a glacial-interglacial cycle, *Science*, *291*(5508), 1511–1517.
Urban, F. E., J. E. Cole, and J. T. Overpeck (2000), Influence of mean climate change on climate variability from a 155-year tropical Pacific coral record, *Nature*, *407*(6807), 989–993.
van Oldenborgh, G. J. (2005), Searching for decadal variations in ENSO precipitation teleconnections, *Geophys. Res. Lett.*, *32*, L15701, doi:10.1029/2005GL023110.
Vásquez-Bedoya, L. F., A. L. Cohen, D. W. Oppo, and P. Blanchon (2012), Corals record persistent multidecadal SST variability in the Atlantic Warm Pool since 1775 AD, *Paleoceanography*, *27*, PA3231, doi:10.1029/2012PA002313.
Weber, J. N., and P. M. J. Woodhead (1972), Temperature dependence of Oxygen-18 concentration in reef coral carbonates, *J. Geophys. Res.*, *77*(3), 463–473.
Wei, W., and G. Lohmann (2012), Simulated Atlantic multidecadal oscillation during the Holocene, *J. Clim.*, *25*(20), 6989–7002, doi:10.1175/jcli-d-11-00667.1.
Wilson, R., A. Tudhope, P. Brohan, K. Briffa, T. Osborn, and S. Tett (2006), Two-hundred-fifty years of reconstructed and modeled tropical temperatures, *J. Geophys. Res.*, *111*, C10007, doi:10.1029/2005JC003188.
Wilson, R., E. Cook, R. D'Arrigo, N. Riedwyl, M. N. Evans, A. Tudhope, and R. Allan (2010), Reconstructing ENSO: The influence of method, proxy data, climate forcing and teleconnections, *J. Quat. Sci.*, *25*(1), 62–78.
Wittenberg, A. T. (2009), Are historical records sufficient to constrain ENSO simulations?, *Geophys. Res. Lett.*, *36*, L12702, doi:10.1029/2009GL038710.
Wu, H. C., B. K. Linsley, E. P. Dassié, B. Schiraldi, and P. B. DeMenocal (2013), Oceanographic variability in the South Pacific Convergence Zone region over the last 210 years from multi-site coral Sr/Ca records, *Geochem. Geophys. Geosyst.*, *14*(5), 1435–1453, doi:10.1029/2012GC004293.
Yasunaka, S., and K. Hanawa (2011), Intercomparison of historical sea surface temperature datasets, *Int. J. Climatol.*, *31*(7), 1056–1073, doi:10.1002/joc.2104.
Zinke, J., W.-C. Dullo, G. Heiss, and A. Eisenhauer (2004), ENSO and Indian Ocean subtropical dipole variability is recorded in a coral record off southwest Madagascar for the period 1659 to 1995, *Earth Planet. Sci. Lett.*, *228*(1), 177–194.
Zinke, J., M. Pfeiffer, O. Timm, W.-C. Dullo, D. Kroon, and B. Thomassin (2008), Mayotte coral reveals hydrological changes in the western Indian Ocean between 1881 and 1994, *Geophys. Res. Lett.*, *35*, L23707, doi:10.1029/2008GL035634.
Zinke, J., M. Pfeiffer, O. Timm, W.-C. Dullo, and G. Brummer (2009), Western Indian Ocean marine and terrestrial records of climate variability: A review and new concepts on land–ocean interactions since AD 1660, *Int. J. Earth Sci.*, *98*(1), 115–133.